1964

Scintillation in the Ionosphere

M. Patrick McCormick
College of William & Mary - Arts & Sciences

SCINTILLATION IN THE IONOSPHERE

A Thesis

Presented to

The Faculty of the Department of Physics

The College of William and Mary in Virginia

In Partial Fulfillment

Of the Requirements for the Degree of

Master of Arts

By

Michael Patrick McCormick

May 1964

APPROVAL SHEET

This thesis is submitted in partial fulfillment of

the requirements for the degree of

Master of Arts

Michael P. McCormick
Author

Approved, May 1964:

James D. Lawrence, Jr., Ph.D.

Melvin A. Pittman, Ph.D.

Donald E. McLennan, Ph.D.

F. R. Cromfield, Jr.

ACKNOWLEDGMENTS

The author wishes to express his appreciation to Dr. J. D. Lawrence, Jr., under whose direction this research was performed, for his untiring guidance and advice. The writer is also indebted to the Physics Department of the College of William and Mary for a fellowship and teaching grants over the last two years. Finally, the author wishes to express a special thanks to his wife, Judy, for her constant aid and encouragement and for typing the manuscript.

TABLE OF CONTENTS

LIST OF FIGURES

ABSTRACT

The design of a receiving station for recording phase fluctuations received from orbiting earth satellites is discussed. The equipment and theory of operation are presented. In order to provide a thorough study, simultaneous amplitude and phase fluctuations are necessary; therefore, the equipment for measuring amplitude scintillation is discussed. A comprehensive comparison of three leading investigators in the field of ionospheric research is presented so that theories can be used in a thorough study of phase and amplitude scintillation. The most recent advances in the knowledge of the ionosphere are ramified.

SCINTILLATION IN THE IONOSPHERE

THE IONOSPHERE

The region of the terrestrial atmosphere between approximately 50 and 500 km is known as the ionosphere. Its upper boundary is not well defined, but its lower one is generally considered to be near 50 km. Figure 1 gives a temperature plot of this region. Note that between 50 and 80 km this region has a negative temperature gradient, but at 80 km the temperature gradient is reversed and the temperature begins to increase with increasing altitude. This increase in temperature of the upper atmosphere is due to strong absorption of ultraviolet radiation from the sun which in turn ionize oxygen and nitrogen giving them high velocities. Low particle densities exist at these altitudes making collision probabilities very small, thus electrons and positive ions have long mean free paths. This keeps them from recombining quickly and the region is ionized continuously and therefore called the ionosphere. It is obvious that it possesses a high degree of electrical conductivity and is an excellent reflector of radio waves. The presence of these free electrons in the ionosphere produce disturbances of radio waves from extraterrestrial sources. The ionosphere is divided, according to height, into the regions called D, E, and F. It was once thought that there were distinct stratifications of electrons in these regions and the levels at which peaks occurred were labeled by these letters. As a result of rocket and satellite measurements,[1-2] it has been found that these layers are not necessarily characterized by a maximum, but are usually marked only by a ledge, where the gradient is small. It will prove convenient, nevertheless, to use the notation,

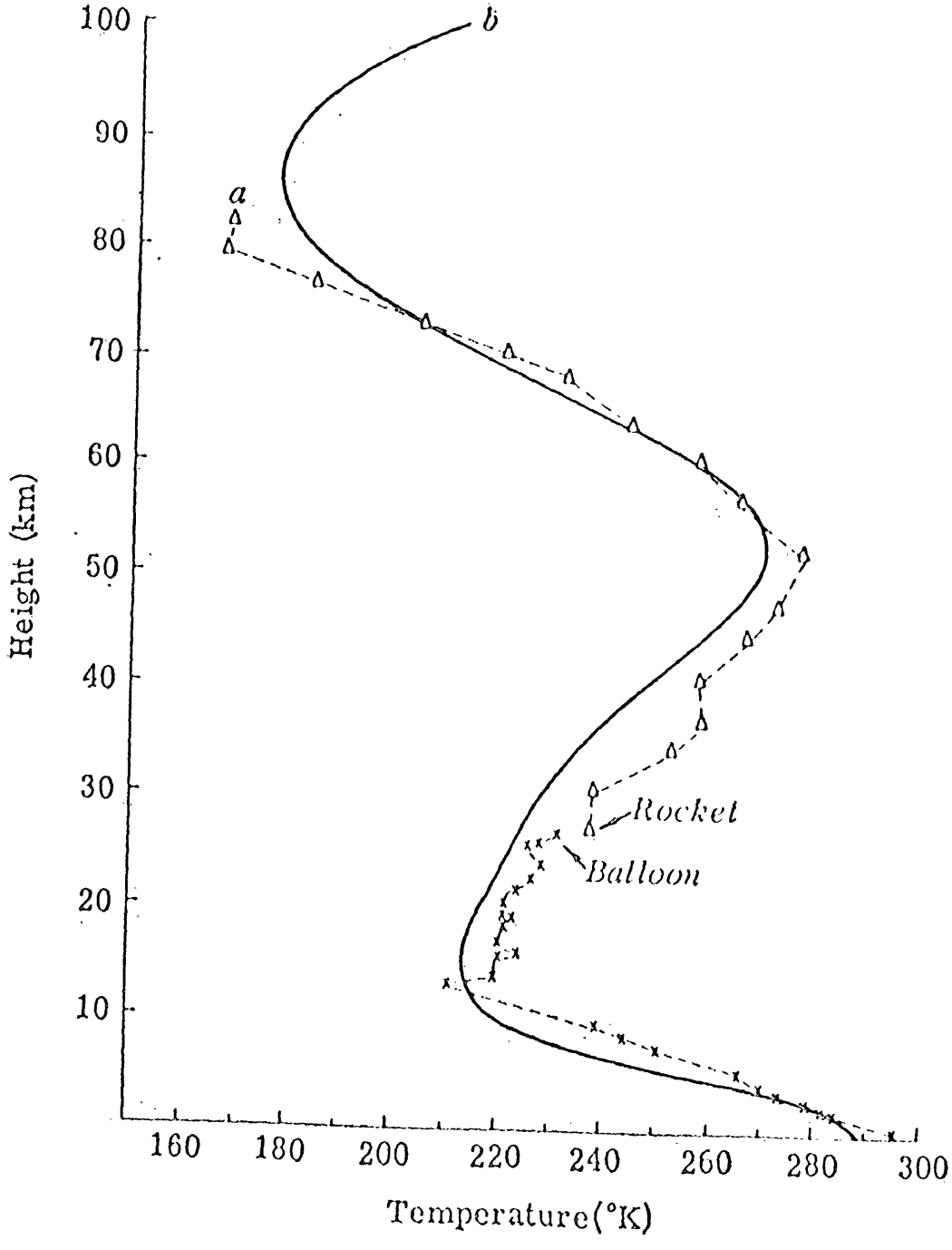

FIG. 1 Temperature as a function of height observed at Fort Churchill, Canada (59°N) at 2330 CST on July 23, 1957 [after W. G. Stroud, W. Nordberg, W. R. Bandeen, F. L. Batman, and P. Titus, *J. Geophys. Research* 65, 2307 (1960)].

E-layer, although its ion density peak may scarcely show a curve if you plot electron density versus height. Figures 2 and 3 are plots of electron density (electrons per cc) versus height (km) for the average daytime ionosphere for the year 1962.

Research in this area of the atmosphere, prior to 1946, was carried out mainly by ionosondes in which radio waves from transmitting stations on the earth are reflected by the ionosphere and received on the earth's surface. The height of the reflecting layer can be found from the time it takes the pulse to return to the ground. There are numerous methods of sounding the earth's atmosphere, but the one almost universally used is the "pulse method" introduced first by Briet and Tuve.[3] Other techniques include observation of noctilucent clouds, auroral studies, and observations of reflections from meteor trails. These techniques, however, are only applicable to the lower portions of the ionosphere below its peak ion density. The top side of the ionosphere was not studied until 1946, when Little and Lovell[4] found that the variation in signal received from a stellar radio source was caused by the local ionosphere. With the advent of artificial earth satellites in 1957, the ionosphere may be more comprehensively studied. Using a satellite as a source has two advantages over a stellar radio source. First, the receiving equipment is simpler due to the coherent radiation and high signal to noise ratio. Secondly, the swift passage of the satellite makes the contribution of the turbulent motion of the ionosphere negligible.

Because there are irregularities of electron density in the ionsophere, a signal emanating from a satellite or radio star exhibits fluctuations in amplitude and phase. Thus, study of the fluctuation or scintillation of satellite or radio star signals is an important

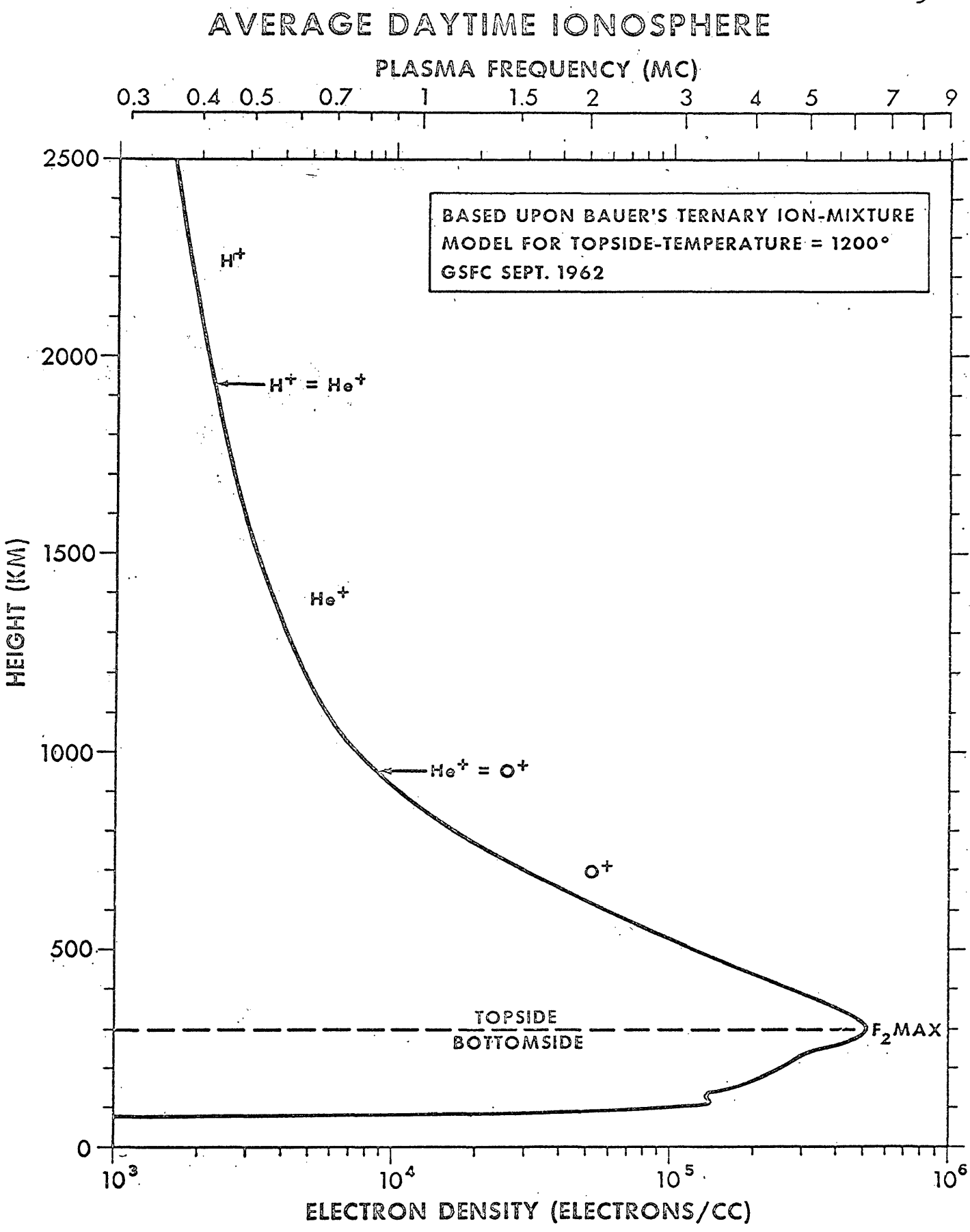
AVERAGE DAYTIME IONOSPHERE
PLASMA FREQUENCY (MC)
0.3
0.4
0.5
0.7
1
1.5
2
3
4
5
7
9
BASED UPON BAUER'S TERNARY ION-MIXTURE
MODEL FOR TOPSIDE-TEMPERATURE = 1200°
GSFC SEPT. 1962
H+
H+ = He+
He+
He+ = O+
O+
TOPSIDE
BOTTOMSIDE
F2MAX
HEIGHT (KM)
2500
2000
1500
1000
500
0
10^3
10^4
10^5
10^6
ELECTRON DENSITY (ELECTRONS/CC)

FIGURE 2

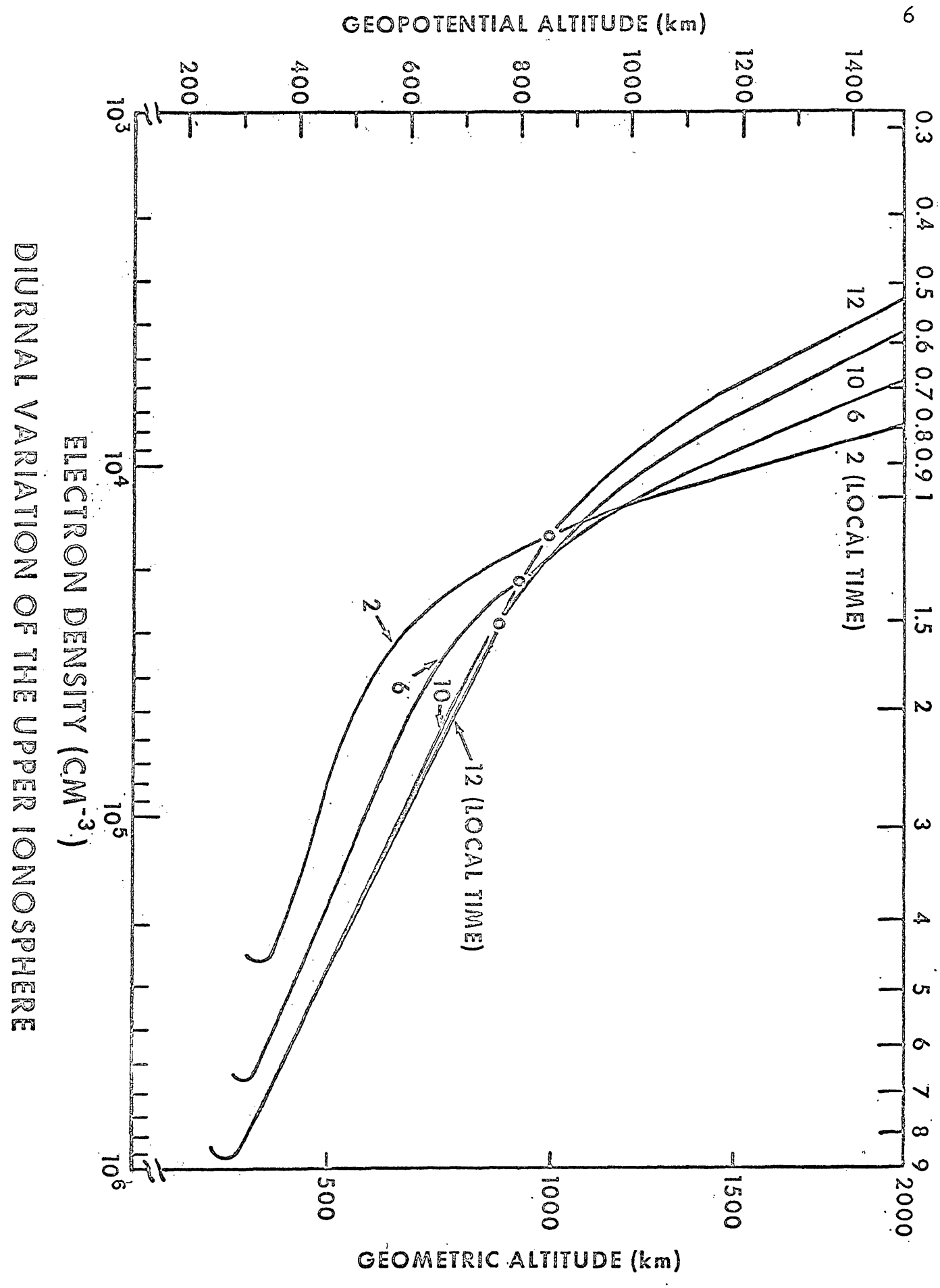

DIURNAL VARIATION OF THE UPPER IONOSPHERE

FIGURE 3

method for studying irregularities of electron density in the ionosphere.

D-Region

The lowest region of the ionosphere is the D-region, generally assigned a height of from 50 to 90 km. Aiken[5] gives the height of maximum density to be about 80 km. This so-called stratification exists only during the daylight hours and merges into the next higher region, the E-region, at night. It then reforms at sunrise. Aiken believes that there is a mechanism responsible for the production, at sunrise, of a two-layered D-region. The first, which he labels D_β, is centered at 73 km and is caused by cosmic rays and photo-detachment from negative ions. This leads to a build up from its nighttime level to its daytime value in about 30 minutes after sunrise. The second layer, which he terms the D_α-region is situated between 80 and 100 km and is formed by attenuated Lyman-alpha ionization of NO. Later in the morning, these two layers then merge into one region. This two-layer model is in agreement with Bracewell's and Bain's[6] explanation of low frequency propagation anomalies at sunrise.

The best experiments to determine the electron content of the D-region have been done by Gardner and Pawsey,[7] and by Fejer.[8] They found the average maximum electron number density to be about 2×10^4 electrons per cc. Nicolet and Aiken[9] have advanced the most detailed analysis of the ionizing radiations in this region to date. They have concluded that the radiations of solar origin penetrating below 85 km are:

(1) X-rays of wavelength less than 10 angstroms

(2) Lyman - α

(3) Wavelengths less than 1800 angstroms

These radiations can ionize:

(1) Molecular nitrogen and oxygen

(2) Nitric oxide

(3) Various atoms such as sodium and calcium

Because the D-region is dependent on solar radiation for its formation, this region often shows sudden large fluctuations in ion density due to solar flares and related solar activities. Sudden ionospheric disturbances (S.I.D.), show that the frequency of occurrence of S.I.D. follows the 11-year solar cycle. These fluctuations are thought to cause polar cap absorptions (P.C.A.) at auroral latitudes, and polar blackouts due to attenuation of electromagnetic waves.

E-Region

The next ionospheric level is situated approximately between 90 and 140 km and is labeled the E-region. The maximum ionization is located at 100 km[10] or 110 km.[11] The average maximum electron number density is usually given as 1.5×10^5 electrons/cc at midday and 1×10^4 electrons/cc at midnight. The coefficient of recombination is usually given as 10^{-8}cc/sec. Wulf and Deming[12] proposed that the chief ionizing process is that of molecular oxygen at its first ionizing potential (12.2 eV). Mitra, Bhor, and Ghosh[13] suggest that the ionization of molecular oxygen at its second ionizing potential (16.1 eV), is responsible. Nicolet[14] has stated that there is a preionization of molecular oxygen due to the strong absorption bands in the energy range 12.2 to 13.55 eV. Bates and Hoyle[15] have proposed a high energy photon theory in which very soft X-radiation is responsible for ionization in this region.

E-layer morphology is influenced slightly by horizontal currents flowing in it across the horizontal geomagnetic field, i.e., the E-layer

acts as a motor. These currents are produced by a dynamo action in the E-region which is due mostly to a diurnal horizontal tidal motion of the conducting medium across a vertical force produced by the terrestrial magnetic field. The current is localized in the E-layer and its variation, during sunspot cycle, is due to the variation in conductivity of the medium.

The E-layer can be considered a Chapman layer given by

$$N = N_o \text{ EXP } \tfrac{1}{2} \left[1 - \frac{Z - Z_o}{H} - \text{SEC } \chi \text{ EXP } \left(-\frac{Z - Z_o}{H} \right) \right]$$

with a scale height H = 10 km, Z_o = 115 km, and $N_o = 2.8 \times 10^5$/cc,[11] α , the recombination coefficient is assumed independent of height.

Many authors modify Chapman's equation in order to explain certain anamolies. Appleton and Lyon[16] state the equation which gives the electron density at any time and height as

$$\frac{\partial N}{\partial t} = q_o \cos \chi - \alpha N^2$$

where α is the recombination coefficient, N the electron density, χ the solar zenith angle at the given time, and q_o the maximum rate of electron (and ion) production for a vertically overhead sun. These equations hold under the condition that

$$\frac{a^2}{2} << 1$$

where

$$a = \frac{\text{TAN } \chi \frac{d\chi}{dt}}{2 \alpha N}$$

The maximum electron density for the E-region slowly builds up at sunrise, from relatively low electron density at night, until it reaches its maximum at about 1300 hours. Note here that this cycle is

not as abrupt as that of the D-region. The critical frequency for this region increases with increasing sunspot number which is another varification of the layer's strong solar correlation.

Sporadic-E

Ionosondes reveal that the critical frequency of the E-region undergoes abrupt and large increases. Regions of intense ionization slightly higher than 100 km have been noted. Because of its sporadic nature, this phenomenon is called "Sporadic-E" or simply E_s. Smith[17] defines sporadic-E as "...comparatively strong and protracted transmission (several minutes to several hours) 'returned' from the E-region of the ionosphere by some mechanism other than the normal reflection process from the daytime regular E-layer."

The most probable radiation sources producing sporadic-E ionization are: high latitude bombardment by high energy protons of solar origin such as those which produce aurora,[18] ionization by winds and turbulence, ionospheric currents, impact by meteors, and thunderstorms.

The structure of the E_s layer is not clear and three models have been proposed to account for experimental observations. These are: (1) patches of thin strata of ionization embedded within the normal E-layer, (2) scattering centers or blobs of ionization of high or low electron density differing from the surrounding portions of the E-region, and (3) a steep gradient in the upper or lower part of the E-layer.

F-Region

The F-region is defined to be the region of the ionosphere above 140 km. The upper boundary is given by Bourdeau[19] to occur where 0+ ceases to be the predominant ion. This region is characterized in the daytime by two ionization peaks. The lower of these, the F_1 peak, has

a maximum ion density located at 160 km with an average maximum electron number density of 2.5×10^5 electrons/cc at midday (at the equator during either equinox).[20] This region can be considered a Chapman layer and the decay of ionization occurs according to a recombination law αN^2, with $\alpha = 8 \times 10^{-9}$cc/sec and the relaxation time of the ionization $(2 \alpha N)^{-1}$ being approximately four minutes. The daily maximum is, therefore, reached a few minutes after midday and is proportional to $\cos^{\frac{1}{2}} \chi$, where χ is the zenith angle of the sun.

Chapman[21] has shown that the absorption of monochromatic solar ionizing radiation in our atmosphere, produces q electrons/cc according to the following

$$q = q_o \exp (1 - z - \sec\chi \, e^{-z})$$

where q_o is the maximum rate of electron (and ion) production for a vertically overhead sun; z is the height above the level of this maximum, measured in units of $H_o = \frac{kT}{mg}$; and χ is the zenith angle at the given time. The electron density at any given time and height is given by the solution of

$$\frac{\partial N}{\partial t} = q - \alpha N^2$$

This theory works fairly well for the F_1 region aside from minor variations or differences, but gives only a crude approximation for the F_2- region.

The F_2-region has a maximum electron density located at 220 km, at the equinoxes, at noon, during sunspot minimum, in moderate to high latitudes, during magnetically quiet days.[20] The average maximum electron number density is given as 5×10^5 electrons/cc and α, the recombination coefficient, is 8×10^{-11}cc/sec in the day and 3×10^{-10}cc/sec at night.

As given before, h_mF_2 (ionization peak of F_2) is 220 km at noon. This value is 10 km lower in winter and 20 km higher in the summer. The midnight value of h_mF_2 is near 320 km with no clear seasonal variation. At the magnetic equator, the F_2 region is higher than at greater latitudes. This is verified at Huancayo where, at noon, h_mF_2 is 350 km and at midnight 300 km. During the sunspot cycle, h_mF_2 rises 30 km at moderate latitudes and 70 km at Huancayo. The F_2-region is perturbed by tidal influences (both solar and lunar), and by conditions produced by magnetic storms. These perturbations, as well as some of the associated anomalies, are due electrodynamical forces associated with the flow of electric currents in the ionosphere.

Since the F_2-region can not be explained by Chapman's law, Bradbury[22] proposed that $\alpha \rightarrow \frac{1}{N}$ for this region and the rate of decay of ionization was βN, where β is an attachment coefficient which decreases with height. This theory explains the variations of maximum electron density with latitude.

Bradbury's method does not, however, explain all of the anomalies. At sunspot maximum, h_mF_2 is higher, while there is little change in h_mF_1. It seems, therefore, that some other reaction contributes to the F_2-region independent of the F_1-region. In order to explain this, Martyn[20] has changed Chapman's law as follows:

$$\frac{\partial N}{\partial t} = q - \beta N - \mathrm{Div}\,(v N)$$

where v is the transport velocity of the electrons. He believes that v can arise in three basic ways: (1) the air in the region may be in motion, carrying the ionization with it; (2) if an electric current is present, the ionization drifts with the velocity vector; (3) the

ionization, under the influence of gravity and its own partial pressure gradient, will diffuse. It has been found experimentally that $h_m F_2$ drifts downward at the magnetic equator at a rate of 19 km/hour. The distinct morphology of the F_2-region is still unexplained, but Martyn has proposed that this is due to changes in the air tides and associated electrodynamic drifts.

The F_2 rise, independent of F_1, can be explained on the basis of heating by semiacoustic waves. Winds and wind gradients are stronger in summer than in winter; therefore, semiacoustic waves are more favorable in summer than in winter causing local heating if absorbed in the more rarefied F_2 region.

The main ionization reactions in the F-region are the ionization of molecular nitrogen from its first (15.5 eV), and second ionization potentials,[12] and the ionization of atomic oxygen from its first, [23-24-25] second and third[26] ionization potentials.

Spread-F

Often ionogram traces of reflections from the F_2-region become broad and diffuse near the critical penetration frequencies. This indicates that this region is anisotropic and can not be considered uniformly stratified. In consequence, it must contain randomly distributed embedded irregularities such as "blobs" or columns of electrons differing from their surroundings. This phenomenon is termed "spread-F". Until recently there has been little doubt that the inhomogeneities associated with spread-F, the magnetic disturbances at mid-to-high latitudes, and the steep gradient at nighttime of ionization of the undersurface of the F-region, are the causes of radio-star and satellite scintillations. Briggs[27] (1964) concluded that radio-star scintillations

could be caused by a region in the ionosphere above h_mF_2. His data are the first to cover a complete solar cycle. He also noted that scintillation is greatest at sunspot maximum while spread-F echoes are greatest at sunspot minimum.

Spread-F occurs mainly at night and at mid-to-high latitudes. It shows a diurnal variation with a maximum frequency of occurrence shortly after midnight. At low latitudes, it seems to occur earlier. At Huancayo, it is most frequent at 2100 hours. The occurrence of spread-F is closely associated with geomagnetic activity. At mid-to-high latitudes, the correlation is strong, but negative. At 35° geomagnetic latitude, there seems to be a minimum of spread-F at all times. Spread-F and radio scintillation occur mainly:

(1) during the night because of the steep ionization gradient of the undersurface of the F-layer

(2) at low latitudes in the early evening at magnetically quiet times and in the early morning during magnetically disturbed times

(3) mid-to-high latitudes during times of magnetic disturbances

S. Rangasivamy and K. B. Kapasi[28] have suggested that a significant lunar variation is observed in the occurrence of low-latitude spread-F which suggests that electrodynamic drift plays an important role in the occurrence of equatorial spread-F.

DISCUSSION OF THEORY

This section presents the methods and findings of Booker, Briggs and Parkin, and Yeh who have made substantial contributions to the theory of ionospheric scintillation. A comparision of their theories, models, derivations, and consequences thereof are discussed in the sections to follow.

Briggs and Parkin,[29] at the University of Adelaide, have examined the variation of radio star and satellite scintillation with zenith angle. They assume that irregular phase fluctuations are impressed on the wave in traveling through the ionosphere and that the amplitude fluctuations develop by a diffraction process as the wave propagates in the free space beneath the ionosphere. They suggest that two effects are produced by increasing the zenith angle of the source. First, the magnitude of the phase perturbations increases because the thickness of the ionosphere increases along the line of sight; and secondly, the geometry of the diffraction process changes. Only amplitude scintillations were actually treated by Briggs and Parkin.

It is assumed that the correlation function of electron density has the form of an ellipsoid of revolution with its long axis along the direction of the magnetic field and that the variation of the correlation function along any radius is Gaussian. From this model, a derivation of the correlation function of phase is made showing that the phase pattern is anisotropic, the contours of equal correlation being ellipses with an axial ratio related to the axial ratio of the blobs. Finally, a derivation of the root mean square deviation of phase produced by an irregular medium is treated.

It is shown that a weighting function for the effectiveness of irregularities in producing amplitude scintillation at different heights from the observer is needed. Theoretical results are given assuming isotropic irregularities and also irregularities elongated along the direction of the earth's magnetic field. A brief outline of the theoretical derivation is given below:

Briggs and Parkin assume the correlation function of electron density N to be

$$\rho_N (r,s) = \text{EXP} \left[- \frac{r^2}{r_o^2} - \frac{s^2}{(\alpha r_o)^2} \right]$$

where r and s are a pair of cylindrical coordinates such that s is measured along the magnetic field and r is measured perpendicular to it. r_o measures the distance at which the correlation falls to $\frac{1}{e}$ in a direction transverse to the field, αr_o the corresponding distance along the field and α the axial ratio. An individual blob (the irregular medium is built up by the superposition of electron clouds or blobs in a random arrangement) has an excess electron density

$$\Delta N (r,s) = \Delta N_o \text{ EXP} \left[- \frac{r^2}{r_o^2/2} - \frac{s^2}{(\alpha r_o)^2} \right]$$

N_o being the excess electron density at the center. The size of a single irregularity is taken to be r_o. The phase change in traveling a distance l in the medium, relative to the phase change in traveling the same distance in a uniform medium with the same mean electron density, is given by

$$\varphi = - r_e \lambda \int_o^l \Delta N \, dl$$

From the geometry of the blob and the previous equations, the derivation of the correlation function of phase is

$$\rho_{\varphi}\,(\,\xi,\varkappa\,) = \mathrm{EXP}\,\left[\,-\,\frac{\xi^2}{r_o^{\,2}} - \frac{\varkappa^2}{(\,\beta\, r_o\,)^2}\,\right]$$

where $\beta = (\,\alpha^2 \sin^2 \Psi + \cos^2 \Psi\,)^{\frac{1}{2}}$ which is the axial ratio of the phase pattern.

Chernov[30] has shown that

$$\varphi_o^{\,2} = 4\pi^2\,\frac{\overline{(\,\Delta\,\mu\,)^2}}{\lambda^2}\,L * \int_{-\infty}^{+\infty} \rho_{\mu}\,(\,0,0,\zeta\,)\,d\zeta$$

where φ_o is the root mean square deviation of phase produced in a wave which travels a distance L through the medium in the z direction, and $\rho_{\mu}(0,0,\zeta)$ is the correlation function of refractive index u in the z direction. Substitution gives the root mean square deviation of phase to be

$$\varphi_o = \pi^{\frac{1}{4}}\, r_e\, \lambda\,\frac{(\,\Delta\,N^2\,\Delta h\,\alpha\, r_o\,\sec i\,)^{\frac{1}{2}}}{(\,\alpha^2\,\sin^2\Psi + \cos^2\Psi\,)^{\frac{1}{4}}}$$

where i is the wave incident angle, Δh is the thickness of the irregularities, and Ψ is the angle between the magnetic field vector and the z - direction.

This equation simplifies into

$$\varphi_o \rightarrow \lambda\,(\,\mathrm{Sec}\ i\,)^{\frac{1}{2}}\,(\,\alpha^2\,\mathrm{Sin}^2\Psi + \mathrm{Cos}^2\Psi\,)^{-\frac{1}{4}}$$

...Eq. (1)

since the irregularities are assumed to have similar statistical properties everywhere. For isotropic irregularities, i.e., $\alpha = 1$,

$$\varphi_o \rightarrow \lambda\,(\,\mathrm{Sec}\ i\,)^{\frac{1}{2}}$$

...Eq. (2)

The scintillation depth is given as

$$S^2 = \frac{\overline{R^4} - \overline{R^2}^2}{\overline{R^2}^2}$$

where R is the amplitude of the wave. Mercier[31] has shown that if φ_o is small

$$S = \sqrt{2}\,\varphi_o \left(1 + \frac{\pi^2 r_o^4}{4 \lambda^2 z^2} \right)^{-\frac{1}{2}}$$

...Eq. (3)

z being the distance from the screen to the observer. Combining Equations 2 and 3 gives

$$S \to \lambda \left(\operatorname{Sec} i \right)^{\frac{1}{2}} \left(1 + \frac{\pi^2 r_o^4}{4 \lambda^2 z^2} \right)^{-\frac{1}{2}}$$

where from the geometry (see Figure 4)

$$i = \operatorname{Sin}^{-1} \left\{ \frac{R_o \operatorname{Sin} \theta}{R_o + h} . \right\}$$

$$z_1 = \left(R_o^2 \operatorname{Cos}^2 \theta + 2 R_o h + H^2 \right)^{\frac{1}{2}} - R_o \operatorname{Cos} \theta$$

$$z_2 = \left(R_o^2 \operatorname{Cos}^2 \theta + 2 R_o H + H^2 \right)^{\frac{1}{2}} - \left(R_o^2 \operatorname{Cos}^2 \theta + 2 R_o h + h^2 \right)^{\frac{1}{2}}$$

where R_o is the radius of the earth, H the height of the satellite above the earth, h the height of the irregularities, z the slant distance between the irregularities and the satellite, and θ the zenith angle.

If we redefine z by $\frac{1}{z} = \frac{1}{z_1} + \frac{1}{z_2}$ the results above may be used for a satellite or radio star. When the source is a satellite

$$S \to \lambda \left(\operatorname{Sec} i \right)^{\frac{1}{2}} \left[1 + \frac{\pi^2 r_o^4 \left(z_1 + z_2 \right)^2}{4 \lambda^2 z_1^2 z_2^2} \right]^{-\frac{1}{2}}$$

Applying this theory, including anisotropic irregularities, the curves for different α, with r_o assumed to be a kilometer, gives a maximum

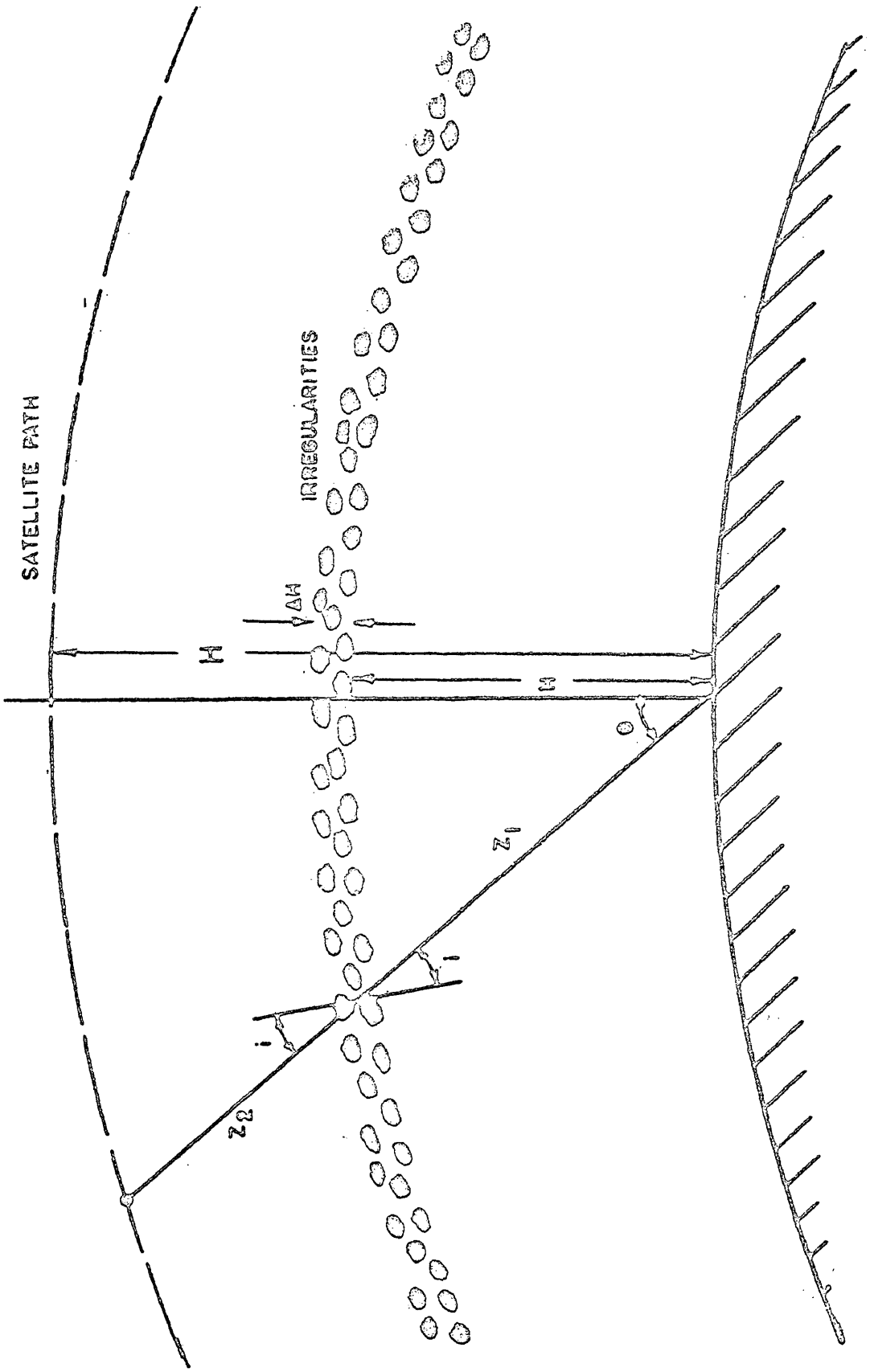

FIGURE 4 — ZENITH ANGLE — SLANT RANGE GEOMETRY

of scintillation depth at 33° north zenith angle in the magnetic meridian plane. Thus the scintillation depth is a maximum when the blobs are viewed end on. This is easier to see when we examine Equation 1.

$$\varphi_o \rightarrow \lambda \left(\text{Sec } i \right)^{\frac{1}{2}} \left(\alpha^2 \text{Sin}^2 \Psi + \text{Cos}^2 \Psi \right)^{-\frac{1}{4}}$$

When the blobs are viewed end on, $\Psi = 0$; therefore, φ_o is greatest. Thus S, which is proportional to φ_o, also increases.

When the waves are received from a satellite

$$\mathcal{Z} = \frac{\mathcal{Z}_1 \mathcal{Z}_2}{\mathcal{Z}_1 + \mathcal{Z}_2}$$

If $\mathcal{Z}_1$ or $\mathcal{Z}_2 = 0$, $\mathcal{Z}$ is zero, and the irregularities close to the observer or very close to the satellite produce only phase scintillations. The maximum value of $\mathcal{Z}$ in Equation 3 occurs when $\mathcal{Z}_1$ equals $\mathcal{Z}_2$, so that the most effective irregularities for the production of amplitude scintillation are those situated halfway between the observer and the satellite. Because of this, a weighting function is derived and should be used.

Yeh,[33] at the University of Illinois, has treated the propagation of spherical waves through an ionosphere containing anisotropic random irregularities. He has followed closely the derivations given by Karavainikov[34] at Moscow. The inductive permeability of the medium is assumed to be that of free space, but the dielectric constant is assumed to be a random variable of the position. The assumption is made that the random irregularities are weak; therefore, ϵ can be used as an expansion parameter. Consequently the problem is the diffraction of a spherical wave by a slab consisting of random irregularities. Since the irregularities are so weak, only single scattering is considered. Yeh

introduces the scalar Helmholtz wave equation and applies first-order perturbation theory showing that the solution is expressible in terms of a series in which the zeroth-order term is the solution in the absence of the irregularities, which would be the familar spherical wave solution. The effect of the wave being scattered once is given by the first-order term and multiple scattering is shown by the remaining higher-order terms. These higher-order solutions may be neglected in a medium whose properties vary sufficiently slowly over one wavelength.

The assumption made is that the autocorrelation function of the dielectric constant is Gaussian with ellipsoidal symmetry. This form was chosen, not randomly, but because experimentally it has been found by many workers that the irregularities in the ionosphere at heights of 300 kilometers are "cigar-shaped" with approximately Gaussian ellipsoidal symmetry. Under this assumption, the mean square deviations and the correlation functions of phase and logarithmic amplitude are derived. The theory is then applied to ionosphere investigations of the dependence of scintillation (phase and logarithmic amplitude) on the height of the satellite source above a layer of irregularities. The theory shows that for temperate and high latitudes the scintillation index is relatively insensitive to the zenith angle of the satellite position. Plots of the theoretical curves suggest the observation of phase scintillation may give data conclusive to finding the height of the region of the irregularities and also the thickness of this region. Yeh's derivations are outlined in the sections to follow. The scalar Helmholtz wave equation, written in normalized units, is

$$\nabla^2 \Psi + [\, 1 + \epsilon \mu(x) \,]^2 = 0$$

Note that ϵ, the inductive permeability, is a constant, while the

dielectric constant is considered a random function of position. When the medium is homogeneous, $\epsilon = 0$, and the solution to the Helmholtz wave equation for an isotropic point source yields the well known spherical wave function

$$\Psi_o = \left(\frac{k A_o}{r} \right) \mathrm{Exp} \left(-j r \right)$$

To solve the equation in general, we assume a solution of the form

$$\Psi(\vec{x}) = \Psi_o(\vec{x}) \mathrm{Exp} \{ -j [\epsilon \varphi_I(\vec{x}) + \epsilon^2 \varphi_2(\vec{x}) + \ldots\ldots] \}$$

This is substituted into the wave equation and coefficients of equal powers in ϵ are equated. This results in a chain of equations which can be changed into an inhomogeneous wave equation and solved in the regular manner. The φ's are then given by

$$\varphi_I = \left(\frac{j r}{2\pi} \right) \int_v \frac{\mu(\vec{x}')}{r'R} \mathrm{Exp} [-j(r' + R - r)] d^3\vec{x}'$$

$$\varphi_2 = \left(\frac{j r}{2\pi} \right) \int_v \frac{\mu(\vec{x}')^2 - [\nabla' \varphi_I(\vec{x}')]^2}{r'R} \mathrm{Exp} [-j(r' + R - r)] d^3\vec{x}'$$

R is the distance connecting the scatterer and the observing field point. The weighting function for φ_I is proportional to the percentage change of the refractive index. The weighting function for φ_2 has two terms both of higher order. These have been introduced to take care of multiple scatter. The irregularities are assumed to be so weak that

can be neglected. The wave function is written

$$\Psi(\vec{x}) = \left(\frac{k A_o}{r} \right) \mathrm{Exp} \left(-j r \right) \mathrm{Exp} \left(-j \epsilon \varphi_I \right)$$

which can be written

$$\Psi(\vec{x}) = \frac{k A(\vec{x})}{r} \mathrm{Exp} \{ -j [r + Q(x)] \}$$

Written in this way, A represents the amplitude and Q the phase departure of the waves. Substitution gives

$$Q(x) = \left(\frac{r\,\epsilon}{2\pi}\right) \int_v \frac{\mu(\vec{x}')}{r'R} \operatorname{Sin}(r' + R - r)\, d^3\vec{x}'$$

$$\operatorname{Log}\left(\frac{A}{A_o}\right) = \left(\frac{r\,\epsilon}{2\pi}\right) \int_v \frac{\mu(x')}{r'R} \operatorname{Cos}(r' + R - r)\, d^3\vec{x}'$$

The autocorrelation function is assumed to be

$$\rho_\mu(\vec{x}) = \frac{\langle \mu(\vec{x}_1)\, \mu(\vec{x}_2) \rangle}{\langle \mu^2 \rangle}$$

where $\vec{x} = \vec{x}_2 - \vec{x}_1$. The correlation functions become

$$\langle Q(\vec{x}_I)\, Q(\vec{x}_2) \rangle = \frac{r_I r_2 \epsilon^2}{4\pi^2} \langle \mu^2 \rangle \int_{v_I} \int_{v_2} \frac{\operatorname{Sin}(r_I' + R_I - r_I)}{r_I' R_I}$$

$$* \frac{\operatorname{Cos}(r_2' + R_2 - r_2)}{r_2' R_2} \rho_\mu(\vec{x}')\, d^3\vec{x}_I')\, d^3(\vec{x}_2')$$

and

$$\langle S(\vec{x}_I)\, S(\vec{x}_2) \rangle = \frac{r_I r_2 \epsilon^2 \langle \mu^2 \rangle}{4\pi^2} \int_{v_I} \int_{v_2} \frac{\operatorname{Cos}(r_I' + R_I - r_I)}{r_I' R_I}$$

$$* \frac{\operatorname{Cos}(r_2' + R_2 + r_2)}{r_2' R_2} \rho_\mu(\vec{x}')\, d^3(\vec{x}_I')\, d^3(\vec{x}_2')$$

The mean square values of the phase departure and logarithmic amplitude are now derived.

$$\langle Q(0,0,z)^2 \rangle = \frac{\epsilon^2 \langle \mu^2 \rangle}{2} \pi^{\frac{1}{2}} l_z b\left\{I + \frac{\sqrt{\left\{\sqrt{\left[(I+\overline{D_x^2})\,(I+\overline{D_y^2}) - (I-\overline{D}_x\overline{D}_y)\right]}\right\}}}{\sqrt{\left[2(I+\overline{D_x^2})\,(I+\overline{D_y^2})\right]}}\right\} \qquad \text{...Eq. 4}$$

$$\langle S(0,0,z)^2 \rangle = \frac{\epsilon^2 \langle \mu^2 \rangle}{2} \pi^{\frac{1}{2}} l_z b\left\{I - \frac{\sqrt{\left\{\sqrt{\left[(I+\overline{D_x^2})\,(I+\overline{D_y^2}) - (I-\overline{D}_x\overline{D}_y)\right]}\right\}}}{\sqrt{\left[2(I+\overline{D_x^2})\,(I+\overline{D_y^2})\right]}}\right\} \qquad \text{...Eq. 5}$$

where

$$D_x = \frac{4\gamma'(z-\gamma')}{l_x^2 z} \quad ; \quad D_y = \frac{4\gamma'(z-\gamma')}{l_y^2 z}$$

γ' is the distance between transmitter and scatterer. The above equations are plotted in Figure 5 assuming the following values:

$$b = \begin{cases} 50 \text{ km} - |a| & \text{when } -50 \text{ km} \leq a \leq 0 \\ 50 \text{ km} & \text{when } a \geq 0 \end{cases}$$

$c = 300$ km

where a is the distance from transmitter to top of the slab of random irregularities, b is the thickness of these irregularities, and c is the distance from the receiver to bottom of the slab of irregularities.

Three cases are considered: (1) the direction of propagation parallel to the major axis of the irregularities and (2) two cases when the direction of propagation is transverse to it. These cases are plotted noting that because of the symmetry of $\bar{D}_x$ and $\bar{D}_y$ the corresponding scintillation indices in case three are identical to those in case two. γ' is assumed to be measured from the transmitter to the center of the slab. This plot of the scintillation index versus height of the transmitter above the top of the slab shows the scintillation index of amplitude varies monotonically as a function of the height, while the scintillation index of phase rises rapidly when the transmitter is inside the slab reaching a maximum near the top of the slab and then decays slightly above the slab. It is thus seen that a determination of the height of the bottom, top, and thickness of the slab can be made by a measurement of the phase scintillation index. This plot also shows that for a constant thickness slab, there exists more scintillation in the longitudinal case (case one) than in the transverse case (cases two and three). Since the effective thickness of the ionosphere varies according to the secant of the zenith angle of the direction of propagation, the effect of increase in scintillation for the longitudinal case should be smaller at the University of Illinois, dip angle 71.3°. In other words, the increase in scintillation with increased zenith angle should balance the increase in scintillation with

longitudinal propagation and the result being that the scintillation index should not change appreciably with zenith angle of the transmitter at high and temperate latitudes. It must be noted, however, that the scintillation depth increases more rapidly with zenith angle than it does with the secant of the zenith angle, thus there is more to this phenomenon than just a thickness effect.

Booker,[35] at Cornell, reviews the experimental evidence concerning radio star scintillation and the theory that currently has been developed to explain it. The basic methods of observation, such as the observation of shadows by two spaced antennas; the fluctuations in phase difference of signals arising at two spaced receivers by the phase-switching interferometer, and the sweep method (sweeping through 40 to 70 MC/S almost simultaneously), are reviewed. The frequency, diurnal, seasonal, and zenith angle variations of amplitude scintillation are discussed, along with scintillation rate, phase scintillation, drift and size of irregularities, and the correlation of radio star scintillation and F-region and E-region phenomena. The mean square fluctuation in phase difference, assuming the electron density is a function of height only and the irregularities are isotropic, and the total mean square deviation of phase introduced by the entire ionosphere are derived. An equation for fluctuation in the direction of arrival of the phase front is also derived. Multiple scattering is neglected in all derivations. The mechanism for producing amplitude and phase scintillation is assumed to be one of scattering. It is expected, therefore, that the remnant of the unscattered wave and waves scattered by various irregularities will be received below the ionosphere. It is noted that both a diffraction theory (Briggs, Yeh) and a scattering theory (Booker) yield the same results. For completeness, the derivations of the theory are developed

below. The plasma wavelength is given as

$$\lambda_N^2 = \frac{\pi}{r_e N}$$

and the refractive index as

$$n^2 = 1 - \frac{\lambda^2}{\lambda_N^2}$$

The mean square deviation of phase introduced by the entire ionosphere is

$$\overline{(\Delta\varphi)^2} = 2r_e^2 \lambda^2 \int_L \overline{(\Delta N)^2}\, dz$$

Introducing the zenith angle and assuming only a certain thickness τ of ionosphere is important in causing phase deviations, this becomes

$$\overline{(\Delta\varphi)^2} = 2r_e^2 \lambda^2 \sec\chi \, L \, \overline{(\Delta N)^2}\, \tau$$

Thus the mean square phase fluctuation is proportional to the secant of the zenith angle and the square of the wavelength at the height where phase scintillations are produced.

This, however, is not what is measured in practice since this gives the phase fluctuation compared to the phase it would have in the absence of fluctuations. What is actually measured is the fluctuations in the phase difference between two antennas separated by a distance d. We assume there is a correlation between them, ρ , and the direction of the source is perpendicular to the separation of the antennas. The mean square fluctuation in phase difference becomes

$$\overline{\{\Delta(\varphi_1 - \varphi_2)\}^2} = 2(1 - \rho)\,\overline{(\Delta\varphi)^2}$$

where $\rho = \exp\left(-\frac{d^2}{L^2}\right)$. Since d is much smaller than L, the scale height,

$$\overline{\{\Delta(\varphi_1 - \varphi_2)\}^2} = 2\left(\frac{d}{L}\right)^2 \overline{(\Delta\varphi)^2}$$

$$\overline{\{\Delta(\varphi_I - \varphi_2)\}^2} = 4r_e^2 d^2 \lambda^2 (\text{Sec}\chi) \frac{I}{L} \overline{(\Delta N)^2} \tau$$

or

$$\overline{\{\Delta(\varphi_I - \varphi_2)\}^2} = \frac{r_e^2 d^2 \lambda^2}{\pi^2} (\text{Sec}\chi) \int \frac{I}{L} \overline{(\Delta N)^2} \, dh$$

...Eq. 6

The mean square variation in direction of arrival becomes

$$\overline{\theta^2} = \frac{r_e^2 \lambda^4}{\pi^2} (\text{Sec}\chi) \frac{I}{L} \overline{(\Delta N)^2} \tau$$

or

$$\overline{\theta^2} = \frac{r_e^2 \lambda^4}{\pi^2} (\text{Sec}\chi) \int \frac{I}{L} \overline{(\Delta N)^2} \, dh$$

Note that the root mean square angular deviation is proportional to the square root of the secant of the zenith angle and the square of the wavelength measured at the level where phase scintillations are imposed.

Assuming single scatter and that the wave is not substantially weakened in traveling through the ionosphere, we may write the relationship

$$\left(\frac{\Delta A}{A}\right)^2 = \overline{(\Delta\varphi)^2}$$

where A is the wave amplitude. $\overline{(\Delta\varphi)^2}$ must be less than unity for this expression to hold (multiple scatter if it is not). Each scatterer is at a distance large compared to the Fresnel zone distance

$$Z_F = \frac{(2\pi L)^2}{\lambda}$$

Under these circumstances, an independent calculation of the mean square fractional deviation of amplitude can be made and should yield the expression already derived for the mean square fluctuation of phase.

Consider the equation for the power scattered within the cone angle measured per unit incident power density, per unit volume, and per unit solid angle

$$\sigma_F = \frac{I}{\lambda} \left(\frac{2\pi L}{\lambda} \right)^3 \overline{\left(\frac{\Delta n}{n} \right)^2}$$

The scattering volume, assuming forward scatter within the small cone angle is

$$V = \pi r^2 \left(\frac{\lambda}{2\pi L} \right)^2 \mathrm{Sec}\chi$$

The scattered power received for an incident power density of p, is

$$p \sigma_F V \frac{S}{r^2}$$

where S is the antenna aperture area. If there are no irregularities, the power received by the antenna would be

$$pS$$

This ratio is the mean square fractional deviation at the receiver

$$\overline{\left(\frac{\Delta A}{A} \right)^2} = \frac{\sigma_F V}{r^2} = 2r_e^2 \lambda^2 \mathrm{Sec}\chi \, L \, \overline{\left(\Delta N \right)^2}$$

or

$$\overline{\left(\frac{\Delta A}{A} \right)^2} = 2r_e^2 \lambda^2 \mathrm{Sec}\chi \int L \, \overline{\left(\Delta N \right)^2} \, dh$$

...Eq. 7

for a continuous distribution of scattering layers throughout the ionosphere. Thus the assumption is proven. For $Z < Z_F$

$$\overline{\left(\frac{\Delta A}{A} \right)^2} = \frac{Z^2}{Z_F^2} \overline{\left(\Delta \varphi \right)^2}$$

and

$$\overline{\left(\frac{\Delta A}{A} \right)^2} = \frac{I}{8\pi^4} r_e^2 \lambda^4 \mathrm{Sec}^3\chi \int \frac{h^2}{L^3} \overline{\left(\Delta N \right)^2} \, dh$$

...Eq. 8

An examination of Equations 6, 7, and 8 for phase and amplitude fluctuations

shows that the relative importance of the different levels in the ionosphere are different for amplitude fluctuations than for fluctuations in the phase difference between the arms of an interferometer. It is possible, therefore, for the level in the ionosphere principally responsible for producing amplitude scintillation to be different from that principally responsible for producing angular scintillation.

In order to find an expression for the height at which all scintillation occurs, it is assumed, in spite of what was previously stated, that the levels are the same for amplitude and phase production.

Assuming $z < z_F$

$$h = 4\sqrt{2}\,\pi^2 \frac{L\,d}{\lambda} \cos\chi \left[\frac{\left(\frac{\Delta_A}{A}\right)^2}{\left\{\Delta(\varphi_1 - \varphi_2)\right\}^2} \right]^{\frac{1}{2}}$$

Thus, simultaneous measurements of the amplitude and phase fluctuations, with a knowledge of the scale of the irregularities, should determine the height at which scintillation occurs.

Summary And Consequences Of Predictions

Booker and Briggs agree that scintillation increases with increasing zenith angle. Yeh agrees with this for low latitudes, but states that at temperate or high latitudes there should be no appreciable change in scintillation with zenith angle. Here at William and Mary, (76° 45' W longitude, 37° 17' latitude) Lawrence et al., have found significant variation in scintillation with zenith angle.

All experimenters agree that the scale of irregularities at the level responsible for scintillation is of the order of one kilometer, and that the blobs are elongated along the earth's magnetic field with an axial ratio of five to one. They also seem to agree that the maximum of scintillation occurs near midnight and that in cases of high solar activity, a maximum daytime scintillation occurs, especially in Australia.

Booker and Yeh have noted that there is little seasonal variation in the Northern hemisphere with Booker giving Australian results indicating a maximum at the solstices and a minimum at the equinoxes. Lawrence and Martin,[36] at William and Mary, have found that a seasonal variation does occur, with a maximum centered about the autumnal equinox and no apparent variation during the solstices. Yeh, Booker, and Briggs, assuming that spread-F pehnomena and radio star scintillation occur at a common level, have found that this level should be between 220-300 km. Briggs has recently found that the degree of irregularity of the ionosphere, ΔN, near the level of maximum ionization of the F-layer, is remarkably constant and does not vary with season or solar cycle, thus the critical penetration frequency changes cause variations of occurrence and intensity of spread-F echoes. In this manner, Briggs indicates that the level for causing radio star scintillations might be a little higher than the location of spread-F phenomenon, especially at sunspot maximum, since he found a maximum of scintillation during minimum sunspot activity and vice versa. Although the physical cause of fluctuations in electron density associated with scintillation is uncertain, there is little doubt that some of the other phenomena involving irregularities of electron density in the ionsophere are due to turbulence. Bowles, et al., [37-38-39-40-41] using an incoherent scatter radar technique, have proposed that plasma wave irregularities are generated by a current stream known as the electrojet. The plasma is believed to become unstable and waves are generated in the direction perpendicular to the magnetic field. These waves would move at roughly the speed of sound in the plasma. One of the biggest puzzles in this research is the cause of the midnight maximum. On the basis of solar activity, it should not occur at night, but in the day. Booker has

proposed that since the electromagnetic damping of turbulence is proportional to the ionization density, which is greatest in the day, there could therefore be explained a maximum at night when the electron density is a minimum. However, this has not held up quantitatively. Thus there still has been no explanation for this maximum.

The most important ramification of Briggs' and Parkin's theory is that scintillation activity is a maximum when the slant range of the emitter is twice the slant range of the layer. This is easily seen in his equation

$$S = \sqrt{2}\,\varphi_o \left[1 + \frac{\pi^2 r_o^4}{2\lambda^2} \left(\frac{z_I + z_2}{z_I z_2} \right)^2 \right]^{-\frac{1}{2}}$$

Only phase scintillation is produced when z_1 or z_2 is equal to zero and we have maximum scintillation when $z_1 = z_2$. Lawrence and Martin have shown that for satellite heights of 500 to 550 km, a maximum in scintillation depth is reached which then decreases slightly out to heights of 1550 km. These data, as shown in Figure 6, are for satellite height above the earth and not for slant height as in Briggs' and Parkin's equation. Martin thus chose an arbitrary zenith angle and plotted a normalized scintillation index versus slant range, but no conclusive evidence of a maximum was found. He applied this to several zenith angles without success.

DeBarber[32] shows that phase fluctuations between spaced antennas are equally sensitive to irregularities at all heights, but amplitude fluctuations on the earth are strongly dependent on the height of the responsible irregularities. Irregularities at small heights contribute much less than those of the same intensity occurring at great heights. This is a reasonable statement, since amplitude fluctuation is a manifestation

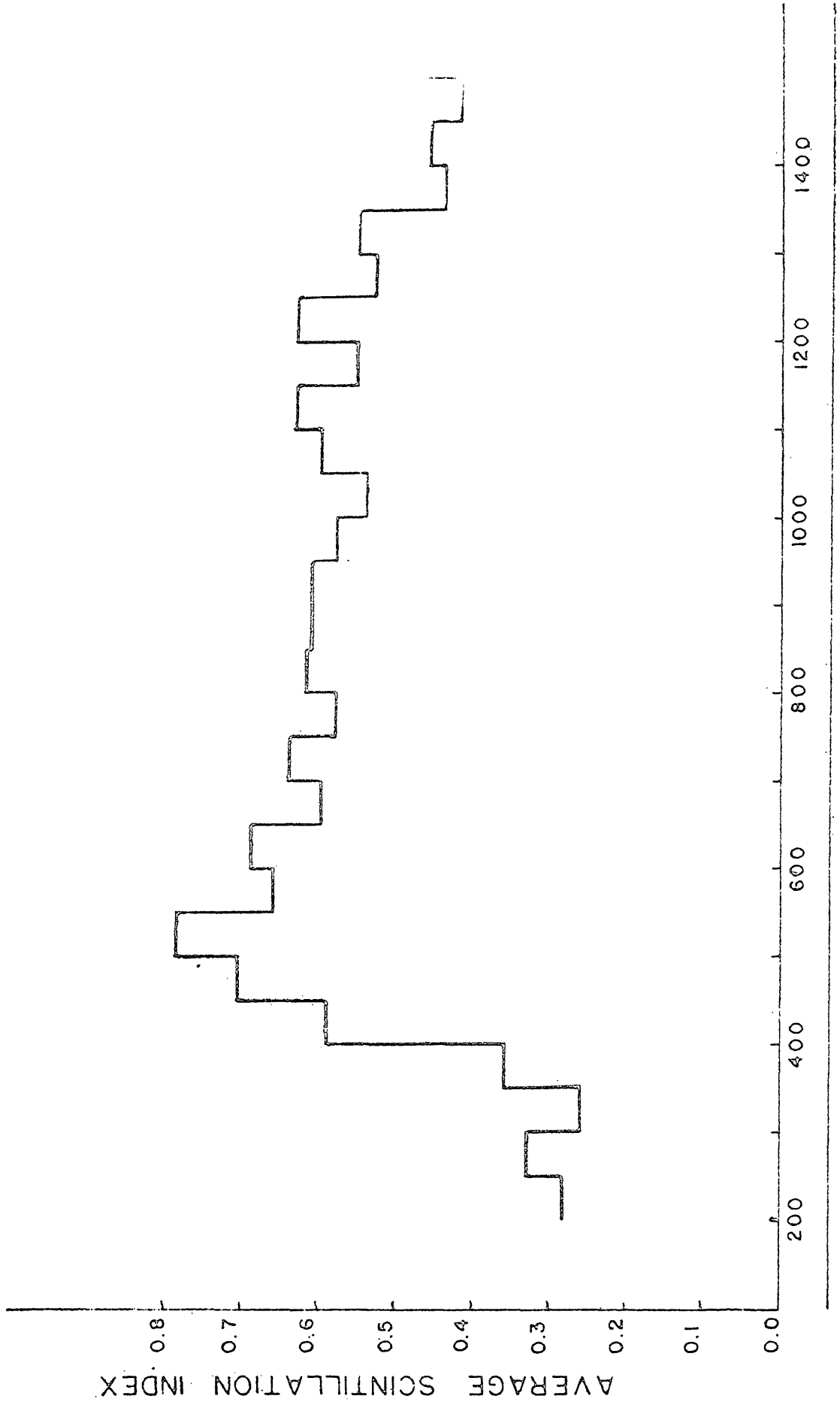

AVERAGE SCINTILLATION INDEX VERSUS HEIGHT FOR COSMOS I, II, V

FIGURE 6

of a diffraction pattern. The waves must travel a distance before a sensible amplitude pattern is formed. Thus, in the Fresnel region, the further the irregularities from the earth, the more intense the pattern.

Yeh has shown theoretically (see Figure 5) using Equation 5 that a maximum for amplitude scintillation should not be found, but that amplitude scintillation should increase monotonically with height of the transmitter. He has shown, however, that there is a maximum found for phase scintillation. Therefore Martin found a maximum for amplitude scintillation which neither theory can explain.

The second most important conclusion found by Briggs' and Parkin's theory is that maximum scintillation is produced when the blobs are viewed end on. Yeh's theory agrees with this as is illustrated in Figure 5 using Equation 4 for case 1. The angle between the line of sight and the magnetic field can be found for any particular zenith angle. The value φ_o and the axial ratio of the phase pattern on the emerging wavefront can be found from

$$\varphi_o \rightarrow \lambda \left(\operatorname{Sec} i \right)^{\frac{1}{2}} \left(\beta \right)^{-\frac{1}{2}}$$

and

$$\beta = \left(\alpha^2 \operatorname{Sin}^2 \psi + \operatorname{Cos}^2 \psi \right)^{\frac{1}{2}}$$

Then we can determine the scintillation depth using

$$S = \sqrt{2}\, \varphi_o \left\{ 1 - \operatorname{Cos} u_I \operatorname{Cos} u_2 \right)^{\frac{1}{2}} \operatorname{Cos} \tfrac{1}{2} \left(u_I + u_2 \right) \right\}^{\frac{1}{2}}$$

where

$$\operatorname{Tan} u_I = \frac{2\lambda z}{\pi r_o^2} \quad ; \quad \operatorname{Tan} u_2 = \frac{2\lambda z}{\pi \beta^2 r_o^2}$$

and

$$z = \frac{z_I z_2}{z_I + z_2}$$

This procedure is then repeated for each value of the zenith angle.

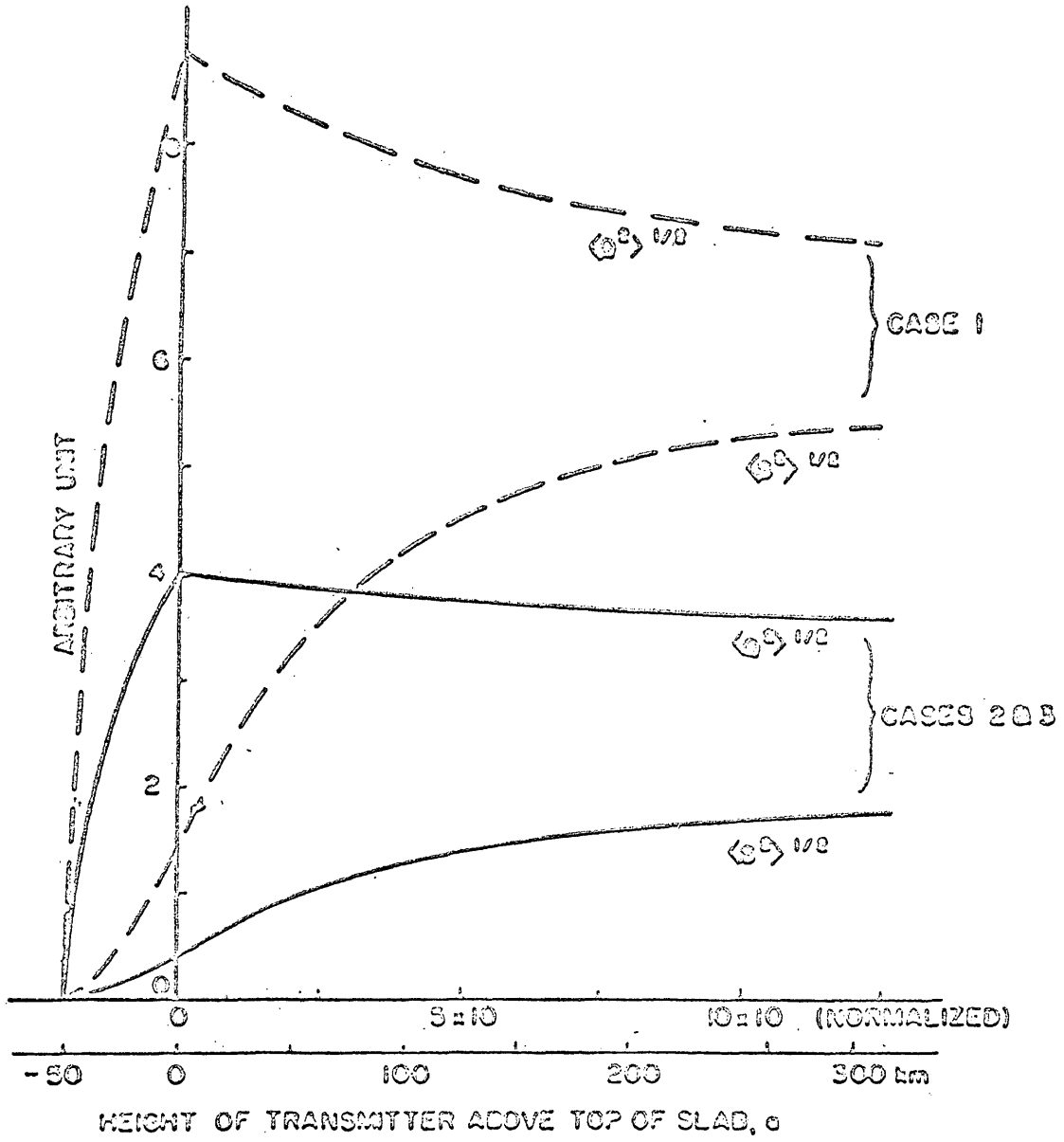

FIGURE 5 *Dependence of scintillation on the height of the transmitter.*

The plot for relative scintillation depth versus zenith angle is given in Figure 7. A peak is given at a zenith angle of 33^{o} towards the North when the irregularities are viewed end on, this being the compliment of the dip angle and thus a peak is noted when the blobs are viewed end on. Note that this peak is superimposed on the normal zenith angle variation.

Here at William and Mary, dip angle 70^{o}, one would expect to observe maximum activity if Briggs' and Parkin's theory was correct; but, no maximum in scintillation activity for latitudes near the receiving station has been found. On the contrary, a distinct minimum was present during periods of substantial scintillation activity. Thus, Briggs' and Parkin's theory does not explain our results.

The most important consequence of Booker's theory comes in the fact that the relative importance of different levels in the ionosphere in producing scintillation is different according to whether the irregularities are large or small compared to their Fresnel zone. He has shown in his theory that each case has its own equation for amplitude fluctuations. Booker also shows that the relative importance of different levels in the ionosphere is different for amplitude fluctuations and for fluctuations in the phase difference between the arms of an interferometer. This can be seen by examining the equations given for $\overline{\left(\frac{\Delta A}{A}\right)^2}$ and $\overline{\{\Delta(\varphi_1-\varphi_2)\}^2}$ noting that their integrals are different.

$$\overline{\left(\frac{\Delta A}{A}\right)^2} = 2r_e^2 \lambda^2 \operatorname{Sec}\chi \int L \overline{(\Delta N)^2}\, dh \quad ; \quad z > z_f$$

$$= \frac{1}{8\pi^4} r_e^2 \lambda^4 \operatorname{Sec}^2\chi \int \frac{h^2}{L^2} \overline{(\Delta N)^2}\, dh \quad ; \quad z < z_f$$

and

$$\overline{\{\Delta(\varphi_1 - \varphi_2)\}^2} = 4r_e^2 d^2 \lambda^2 \operatorname{Sec}\chi \int \frac{1}{L} \overline{(\Delta N)^2}\, dh$$

It is thus possible that the level principally responsible for amplitude

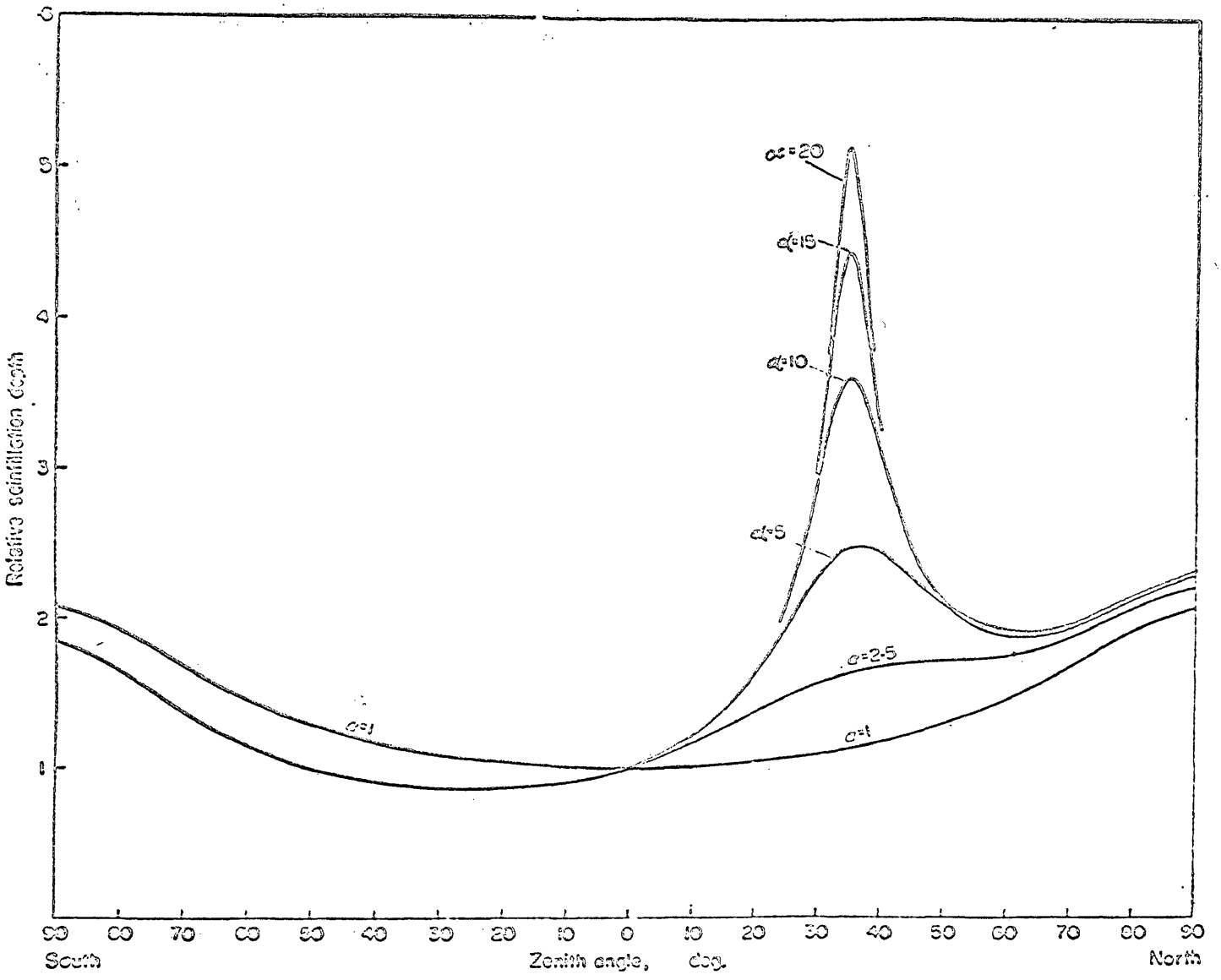

Fig. 7 The zenith angle variation in the magnetic meridian plane for scintillations of the signals from the satellite Explorer VII on 20 Mc/s, observed at Brisbane. The curves are for different values of the axial ratio α, and for irregularities at a height of 300 km. The curves are normalized to unity at the zenith.

scintillations could be substantially different from the level principally responsible for phase fluctuations.

I have thus presented the theories of Briggs and Parkin, Yeh, and Booker, giving their models, assumptions, derivations, and finally concluding with the ramifications and comparisons of the theories of each, including the results of data procured at the College of William and Mary.

All of these theories have been presented assuming a thin layer approximation. The scatter technique of Yeh assumed single scatter which is the same as assuming a thin layer as did Booker, and Briggs and Parkin in their diffraction theories. It is now thought that a thin layer assumption is erroneous since it has been found by many workers that the irregularities responsible for producing fluctuations vary in thickness and in height. Deardon,[42] using radar techniques to study the ionosphere, has found that the layer responsible for producing scintillation is about 150 km thick between a height of about 330 to 450 km above the earth. Bowles[43] has measured electron density profiles as high as 5000 km using his incoherent scatter radar technique. He found the electron density at 5000 km to be about 10^3 electron per cc. Electrojets have been found using rockets[44] at 122 and 128 km and by Bowles at 96-102 km and 102-108 km. These would all produce irregularities that would cause scintillation for which a thin layer model would not give a satisfactory description.

EXPERIMENT

It was my purpose, at the outset of this experiment, to build a device for measuring the deviations of phase between two antennas and to record these fluctuations in phase. Superimposed upon a gradually varying phase difference, resulting from the motion of the satellite, will be a random fluctuation due to the irregularities of electron density in the ionosphere. The station was constructed so that data could be taken that would afford a study of phase and amplitude scintillation simultaneously, giving information concerning the height, thickness, and variations of the irregularities in the ionosphere. Since the S-66 Satellite has failed to orbit, no data have been collected and thus, no results are available. There have been little phase scintillation data procured using this method or any other method, although the literature has concluded that a thorough study of the ionosphere is incomplete without simultaneous phase and amplitude scintillation data.

EQUIPMENT

A block diagram of the phase scintillation receiving and recording equipment is shown in Figure 8. The satellite signal received from two folded dipole antennas are individually beat at the input coil of two Tapetone converters by a common signal generator set at the satellite signal minus 3 KC/S, thus giving a 14.4 MC/S carrier with a 3 KC/S envelope. These signals are then demodulated in separate Collins 51J-4 receivers giving 3 KC signals whose phase difference is then measured by an Ad-Yu phase meter. The output of the phase meter is fed into a biasing system which drops the D.C. level to achieve a differential drive near ground potential and then into a Brush Pen Recording system.

Each of the components of this system will be discussed in the sections to follow.

The amplitude scintillation receiving and recording system is shown in Figure 9. It is to be used in conjunction with the phase equipment so that both phase and amplitude studies can be carried out simultaneously.

Antennas

The antennas used for this experiment are half-wave folded dipoles constructed of heavy duty 300 ohm, twin lead (amphenol 214-185). The length of the half-wave sections in free space is given by

$$d_o = \left(\frac{\lambda_o}{2}\right) = \frac{kcV}{2f} \text{ or } \frac{\lambda_o}{2} = \frac{492 \text{ kV}}{f(\text{MC/S})} = \frac{(492)(0.95)}{40} = 11.68 \text{ ft.}$$

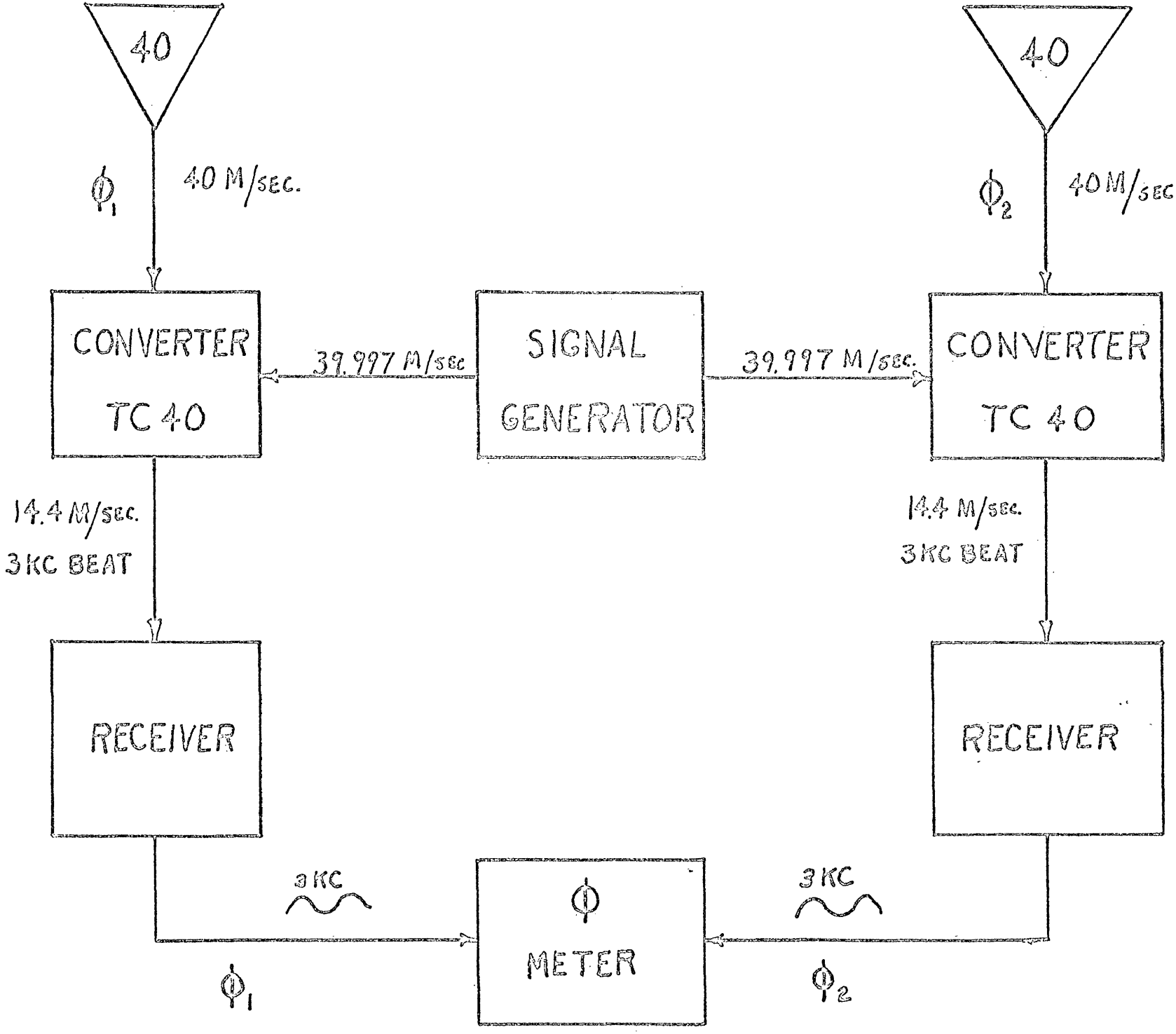
40
40
ϕ_1
40 M/SEC.
ϕ_2
40 M/SEC.
CONVERTER TC 40
39.997 M/SEC
SIGNAL GENERATOR
39.997 M/SEC.
CONVERTER TC 40
14.4 M/SEC. 3KC BEAT
14.4 M/SEC. 3KC BEAT
RECEIVER
RECEIVER
3KC
ϕ METER
3KC
ϕ_1
ϕ_2

FIGURE 8

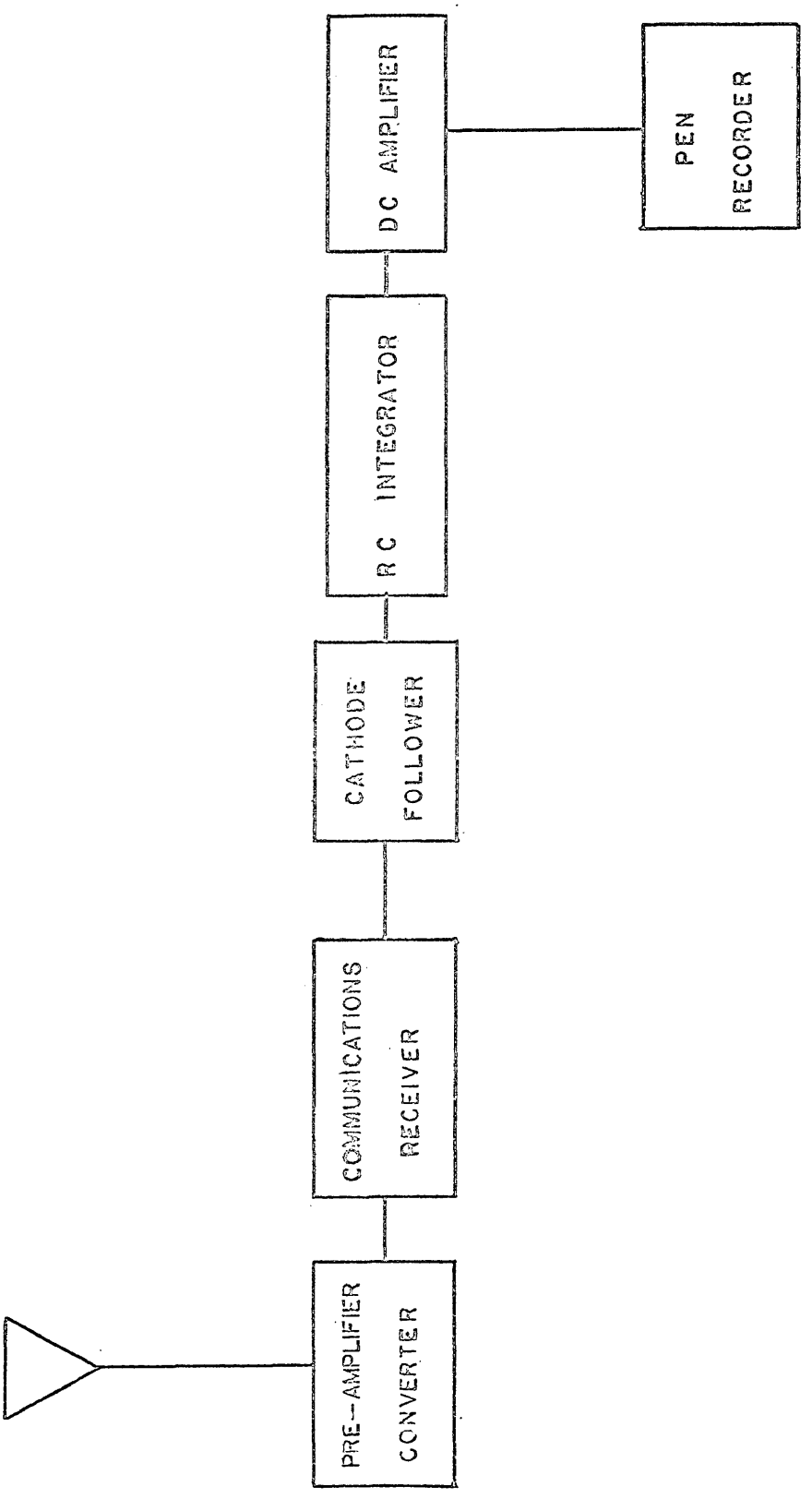

BLOCK DIAGRAM OF RECEIVING EQUIPMENT

FIGURE 9

where c is the velocity of light in free space, k is the end correction factor which is 0.95, V the velocity factor (equal to 1 in free space), and f the frequency. The length of the folded section of the antenna is

$$d_1 = \frac{kcV}{2f} = \frac{(492)(0.84)(0.95)}{40} = 9.82 \text{ ft.}$$

where V, the velocity factor, for 300 ohm twin lead is given as 0.84,

$$d_1 = \frac{\lambda}{2} = 0.84 \frac{kc}{2f}$$

We must therefore add a piece of a heavy copper wire to each end of the antenna correcting for the difference between the total antenna length and the length of the folded section.

$$d_{ew} = \frac{11.68 - 9.82}{2} = 0.93^{28} \text{ ft.} = 11.16 \text{ inches}$$

or

$$d_{ew} = (\frac{1 - 0.84}{2}) \frac{kc}{2f} = 0.9328 \text{ ft.} = 11.16 \text{ inches}$$

Since a 73 ohm transmission line (RG-59/U) was used to connect the (300 ohms) antenna to our receiving equipment, the impedance was matched by means of a 4-to-1 step down balun (see Figure 10). The velocity factor for RG-59/U coaxial cable was taken to be 0.66.[45]

$$d_B = \frac{(492)(0.66)}{40} = 8.12 \text{ ft.}$$

Glass insulators on the ends of the dipoles were connected to $\frac{1}{4}$-inch diameter nylon rope which were fed through pulleys atop 27-feet high aluminum masts and tied at ground level. (This facilitated changing antennas.) The ground plane of the antenna is not known, nor has an artificial one been constructed.

Converters

To convert the satellite signal to an intermediate frequency

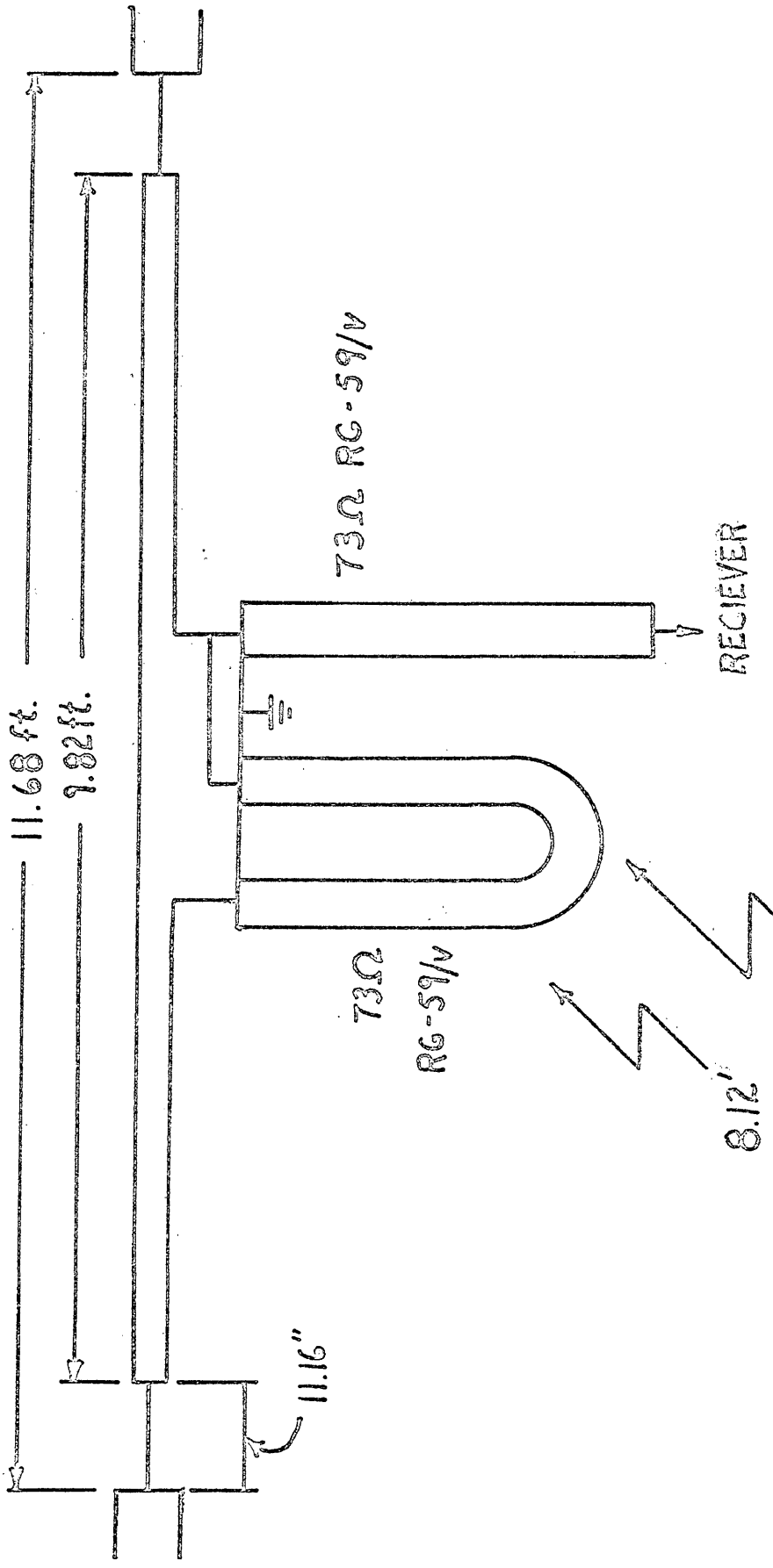

40 MCS FOLDED DIPOLE

FIGURE 10

of 14.4 MC/S, Tapetone TC-series converters were used. The schematic for a TC-40 is shown in Figure 11. They are crystal controlled, employing a pair of 6 BQ7A tubes as a cascade RF amplifier, followed by a mixer stage utilizing a 6CB6 and a 12AT7 in the local oscillator section.

Noise figures for these converters range from 1.5 to 3 db. They have an overall bandwidth of from 1 to 2 MC/S and a power gain of 37 to 44 db. The mixer injection voltage is about 2 volts. The signal generator is coupled by two turns of number 16 wire at input coil L_1.

Receiver

The receivers used for demodulation of the signals were two 51J-4 Collins Communication Receivers. The block diagram for this receiver is shown in Figure 12. These are complete coverage superheterodyne receivers employing single, double, and triple conversion through a range of 540 KC/S to 30.5 MC/S, either AM or CW reception, with a total setting error and drift of less than 1 KC at any frequency within its range. Calibration at room temperature will give frequency stability within 300 C/S and it will operate properly from $-20^{\circ}C$ to $+60^{\circ}C$. Less than 5 uv input gives a 10 db signal to noise ratio.

At 14.4 MC/S, the signal receives one stage of r-f amplification and is then fed to the grid of the first mixer (6BE6) to produce a variable i-f frequency of 2 MC/S by beating with the second harmonic of an 8 MC/S crystal in a high frequency oscillator section. This 2 MC/S signal is combined in the second mixer grid (6BE6) with the 2.5 MC/S, highly stable variable frequency oscillator, to produce a fixed 500 KC/S i-f. It is then amplified in three i-f sections

SCHEMATIC: TC - 40 SATELLITE CONVERTER IF - 14.4 MC.

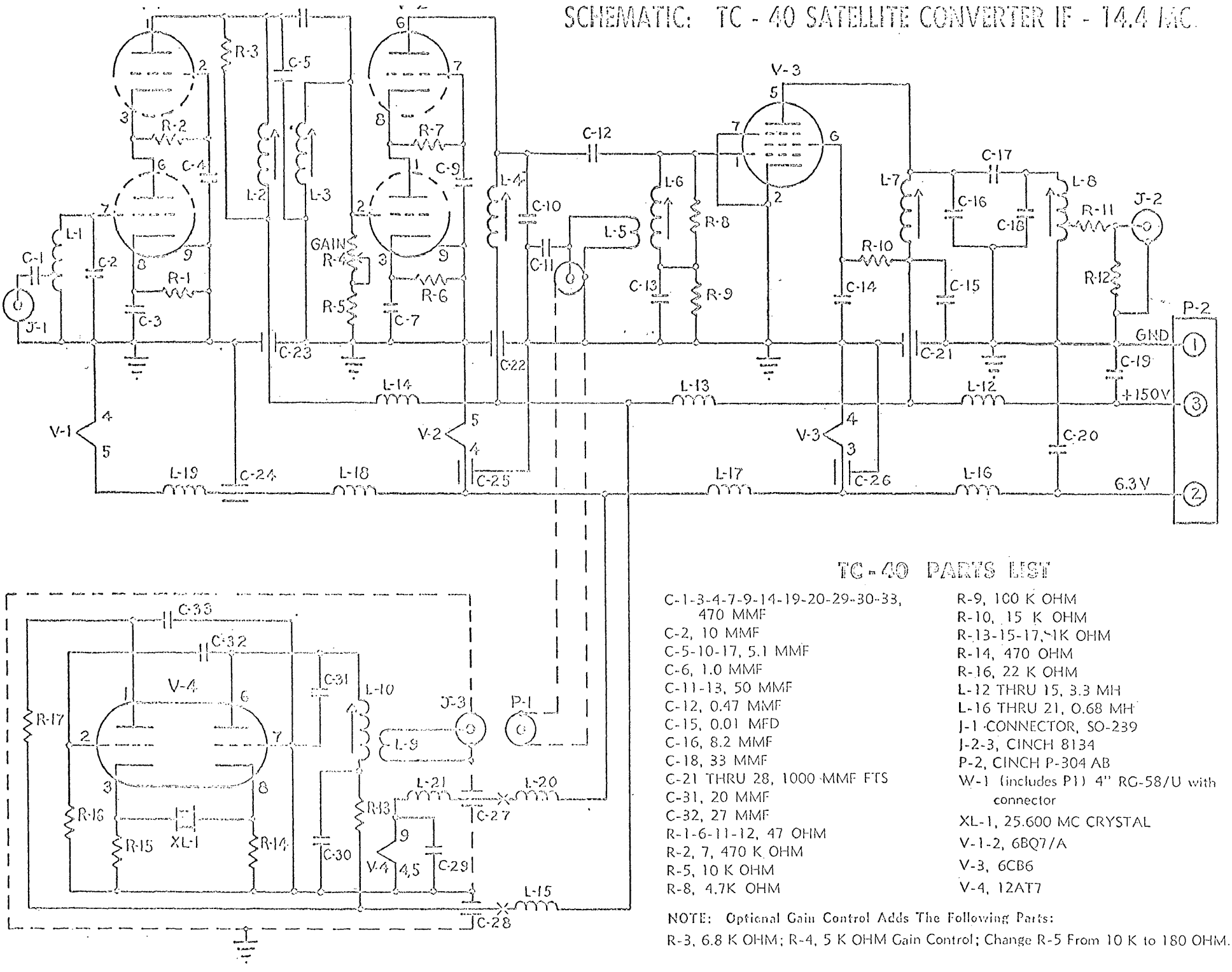

TC-40 PARTS LIST

C-1-3-4-7-9-14-19-20-29-30-33, 470 MMF
C-2, 10 MMF
C-5-10-17, 5.1 MMF
C-6, 1.0 MMF
C-11-13, 50 MMF
C-12, 0.47 MMF
C-15, 0.01 MFD
C-16, 8.2 MMF
C-18, 33 MMF
C-21 THRU 28, 1000 MMF FTS
C-31, 20 MMF
C-32, 27 MMF
R-1-6-11-12, 47 OHM
R-2, 7, 470 K OHM
R-5, 10 K OHM
R-8, 4.7K OHM
R-9, 100 K OHM
R-10, 15 K OHM
R-13-15-17, 1K OHM
R-14, 470 OHM
R-16, 22 K OHM
L-12 THRU 15, 3.3 MH
L-16 THRU 21, 0.68 MH
J-1 CONNECTOR, SO-239
J-2-3, CINCH 8134
P-2, CINCH P-304 AB
W-1 (includes P1) 4" RG-58/U with connector
XL-1, 25.600 MC CRYSTAL
V-1-2, 6BQ7/A
V-3, 6CB6
V-4, 12AT7

NOTE: Optional Gain Control Adds The Following Parts:
R-3, 6.8 K OHM; R-4, 5 K OHM Gain Control; Change R-5 From 10 K to 180 OHM.

FIGURE 11

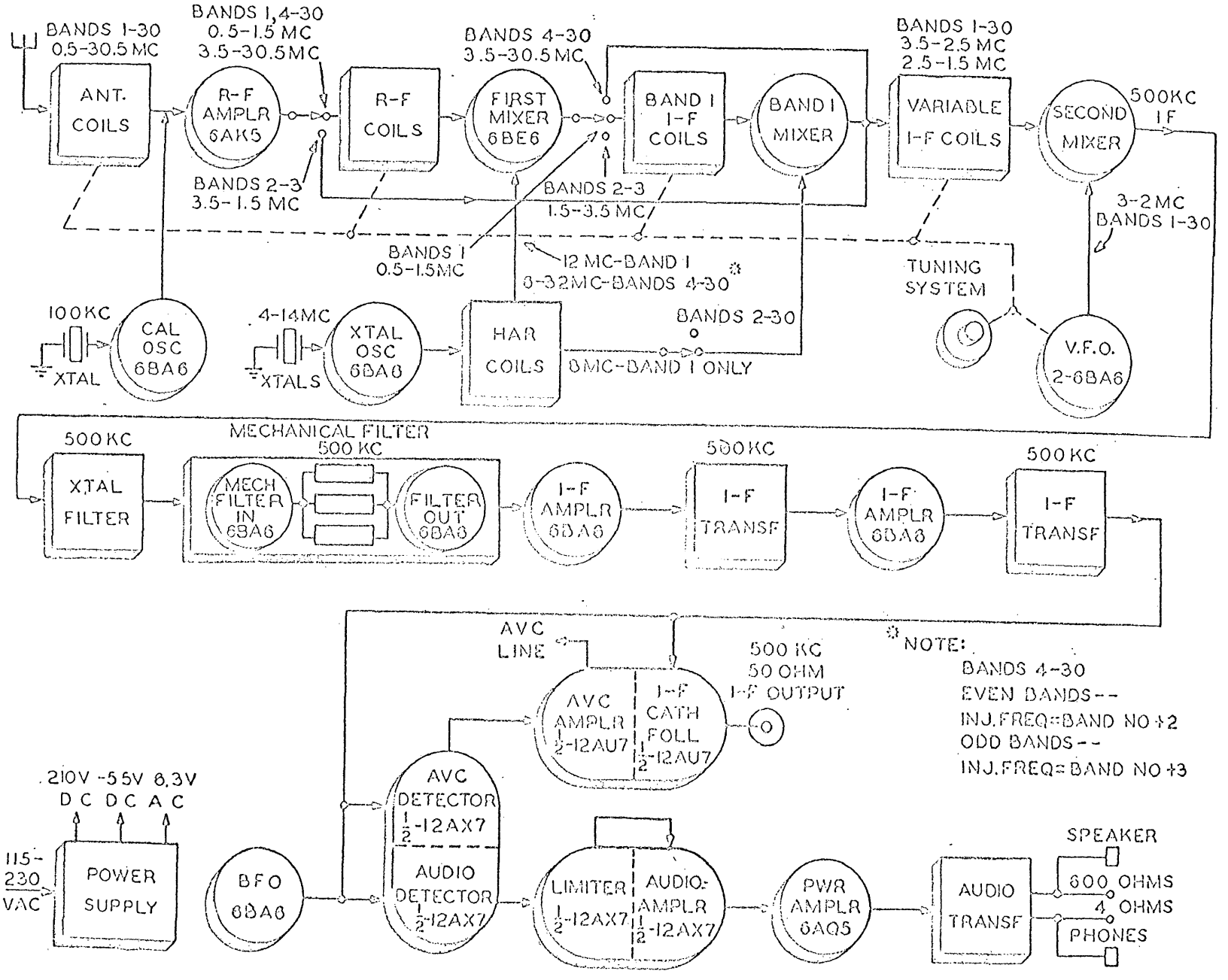
BANDS 1-30
0.5-30.5 MC
ANT. COILS
BANDS 1,4-30
0.5-1.5 MC
3.5-30.5 MC
R-F AMPLR 6AK5
BANDS 2-3
3.5-1.5 MC
R-F COILS
BANDS 4-30
3.5-30.5 MC
FIRST MIXER 6BE6
BAND 1 I-F COILS
BAND 1 MIXER
BANDS 1-30
3.5-2.5 MC
2.5-1.5 MC
VARIABLE I-F COILS
SECOND MIXER
500KC I F
3-2 MC BANDS 1-30
BANDS 2-3
1.5-3.5 MC
BANDS 1
0.5-1.5MC
12 MC-BAND 1
8-32MC-BANDS 4-30
TUNING SYSTEM
100KC
XTAL
CAL OSC 6BA6
4-14MC
XTALS
XTAL OSC 6BA6
HAR COILS
BANDS 2-30
8MC-BAND 1 ONLY
V.F.O. 2-6BA6
500 KC
XTAL FILTER
MECHANICAL FILTER 500 KC
MECH FILTER IN 6BA6
FILTER OUT 6BA6
I-F AMPLR 6BA6
500KC
I-F TRANSF
I-F AMPLR 6BA6
500 KC
I-F TRANSF
AVC LINE
AVC AMPLR ½-12AU7
I-F CATH FOLL ½-12AU7
500 KC 50 OHM I-F OUTPUT
NOTE:
BANDS 4-30
EVEN BANDS--
INJ. FREQ=BAND NO+2
ODD BANDS--
INJ. FREQ=BAND NO+3
210V -55V 6.3V
D C D C A C
115-230 VAC
POWER SUPPLY
BFO 6BA6
AVC DETECTOR ½-12AX7
AUDIO DETECTOR ½-12AX7
LIMITER ½-12AX7
AUDIO AMPLR ½-12AX7
PWR AMPLR 6AQ5
AUDIO TRANSF
SPEAKER
600 OHMS
4 OHMS
PHONES

FIGURE 12

(6BA6's) which follow. The audio output is 0.5 watt for a 5 uv signal, while audio distortion is less than 10% at 0.5 watt output. Other features include a good noise limiter, two stages of audio amplification, a low impedance AVC, and a 100 KC/S calibrator or frequency spotter. Mechanical i-f filters are used to provide bandwidths of 1 KC/S, 3 KC/S, or 6 KC/S. The 6 KC/S mechanical filter is used, passing a band of frequencies approximately 6 KC/S wide centered on the 500 KC/S i-f.

For amplitude studies, the satellite signal is taken from the diode load test point shown in Figure 13 which is in the detector circuit. Due to unknown integration, we must remove the signal at the second detector stage. The signal voltage is then integrated and recorded.

For phase scintillation studies, the satellite signal is taken from the 4 ohm audio output connection at the rear of the receiver.

Biasing System

A biasing system was built to achieve a differential drive near ground potential in order for the signal from the phase meter to be fed to the Brush Recording system (see Figure 14). The power supply provides a regulated voltage of +450 volts and -150 volts with less than 0.1 percent ripple. The rectifier employs 4 IN1732, 2000 PIV, silicon rectifiers in a Graetz Bridge arrangement. This is followed by a π-section filter containing two 10 uf, 1000V, electrolytics and an 8 henry choke, rated at 200 ma. The variable resistors in the balancing section are 1000 ohm precision helipots so that a linear response is obtained.

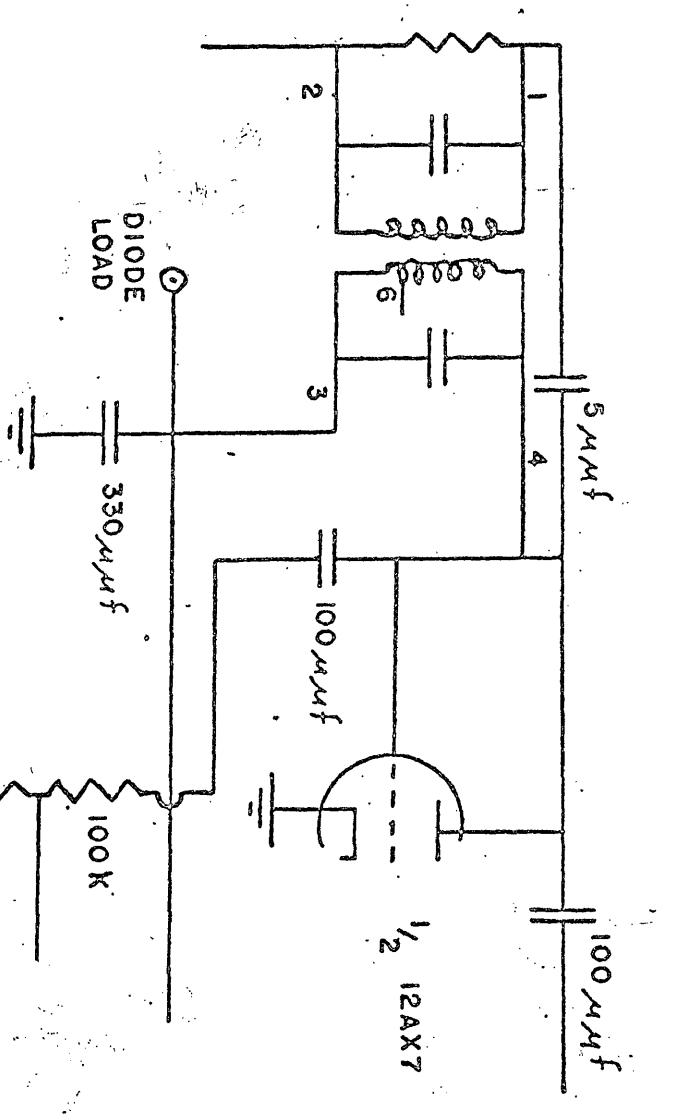

FIGURE 13 COLLINS 51J-4 OUTPUT LOCATION

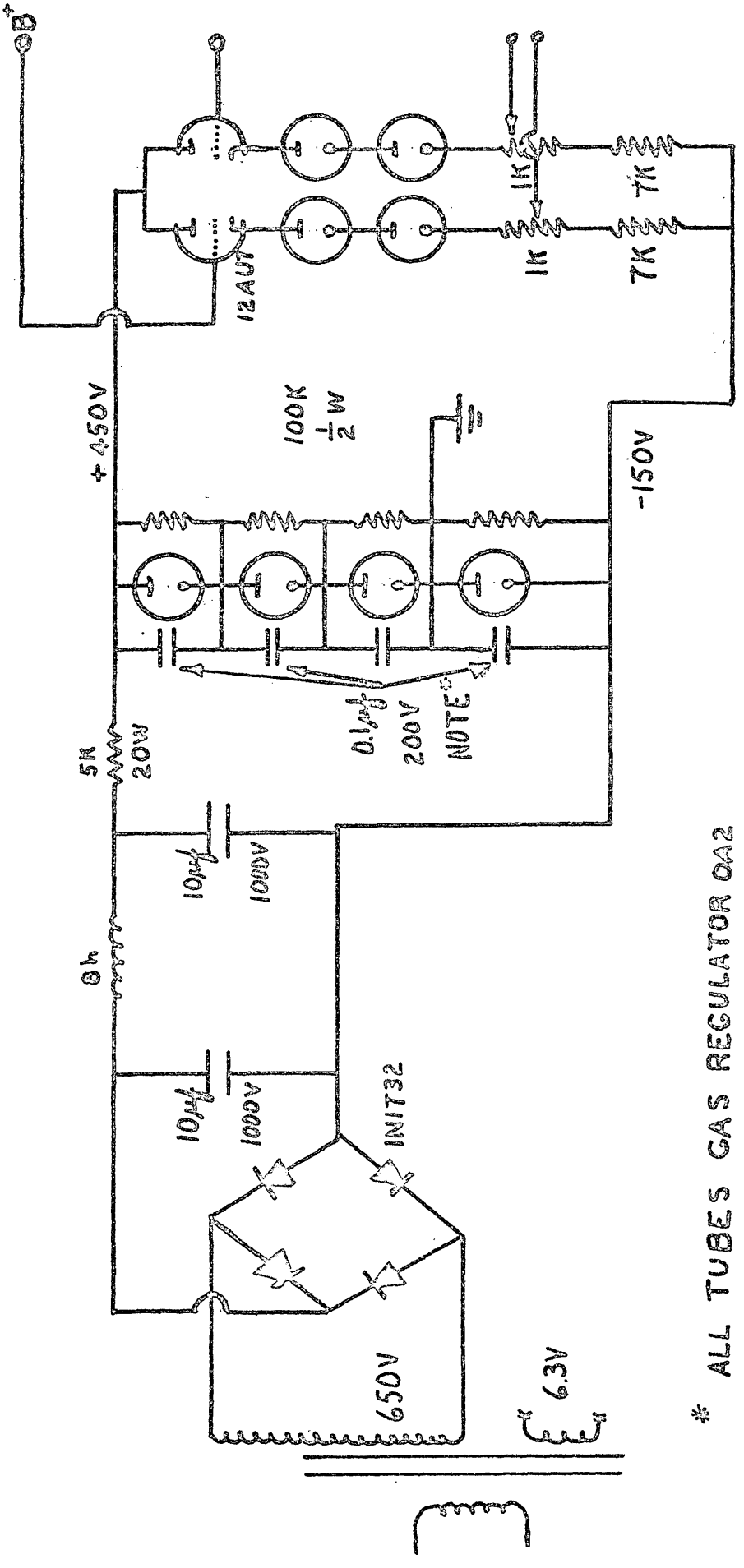

* ALL TUBES GAS REGULATOR OA2

FIGURE 14

Phase Meter

The phase meter for this experiment is an Ad-Yu Type 405. It has a frequency response of from 8 C/S to 40 KC/S which can be increased to 100 KC with increased signal amplitudes and decreased accuracy. There are four phase ranges, G-12, 0-36, 0-90, and 0-180 degrees full scale with a switch provided to add 180 degrees phase shift, in order to obtain ranges of 180-192, 180-216, 180-270, and 180-360 degrees. The relative accuracy (the accuracy of the difference in phase reading from one condition to another) is given as $\pm$ 0.25 degrees, and the absolute accuracy (the accuracy of the phase meter compared to a phase standard) is given as $\pm$ 1 degree or 2% at any range up to 40 KC/S. The input signal voltage can be varied from 0.3 volt to 90 volts rms without affecting the meter reading in the 8 CP/S to 40 KC/S frequency range. From 40 KC/S to 100 KC/S the input voltage must increase to at least 0.5 volt at this highest frequency for no distortion. The D.C. component of the input signal should not be over 400 volts. The meter reading is independent of signal ratios up to 100, and the input impedance of 3 megohms shunted by 20 uu-farads is seen at both input channels. The output signal for external recording is a constant amplitude pulse with repetition rate equal to the input signal frequency and duty cycle proportional to the phase angle between the two input signals. The duty cycle and repetition rate instantly follow any change of input signal frequency and phase angle. Between the meter and the "out" jack an integrating circuit with a time constant of 0.1 second is connected. To record fluctuations of up to 100 C/S, the time constant must be changed to 0.0006 second so that the phase and amplitude are preserved to within five percent. The output impedance at the meter is 3.6 K and after the integrating

circuit is 360 K. The output voltage (B+) is zero for zero degrees and for 180 degrees is -14 volts increasing linearly between these values of phase angle.

Figure 15 shows a block diagram of the phase meter. The input signals E_1 or E_2 are applied to a four-stage cathode-coupled limiter, CL_1 to CL_{14}. A cathode-coupled limiter produces a square wave with its zero voltage axis intersecting points identical to those of the input signal E_1 or E_2. Positive feedback is provided in CL_{14} and C_{24} for decreasing the rise time of the output square wave. Each square wave is fed into a coincident slicer circuit, which is used to activate the panel meter. A complete circuit diagram of the instrument is shown in Figures 16 and 17.

Recording System

The signal from the biasing system is fed to a four-channel Brush Pen Recording system, Model RD-2641-00. This system includes a D.C. amplifier, Model RD-5211-03, which provides sensitivity steps of 0.01, 0.02, 0.05, 0.1, 0.2, 0.5, 1, 2, 5, and 10 volts per chart line (mm) on the oscillograph. The amplification allows from 0.4 volt to 400 volts full-scale measurement and the D.C. sensitivity of the oscillograph pen motor is 1.5 volts per chart line (mm) or 30 volts full scale from center. The frequency response of a recorded peak-to-peak amplitude of a constant voltage sine wave will be within $\pm \frac{1}{2}$ chart line (mm) of a nominal 40 lines from D.C. to 100 C/S. The maximum amplitude is 40 lines (mm) peak-to-peak to 40 C/S. Twenty lines (mm) peak-to-peak to 70 C/S and 10 lines (mm) peak-to-peak to 100 C/S. Chart speed regulation is achieved from a synchronous motor direct drive with paper drift less than $\pm$ 1/3 mm. to record chart speeds of 1, 2, 5, 10, 25, 50, 125, and 250 mm/sec. For amplitude scintillation

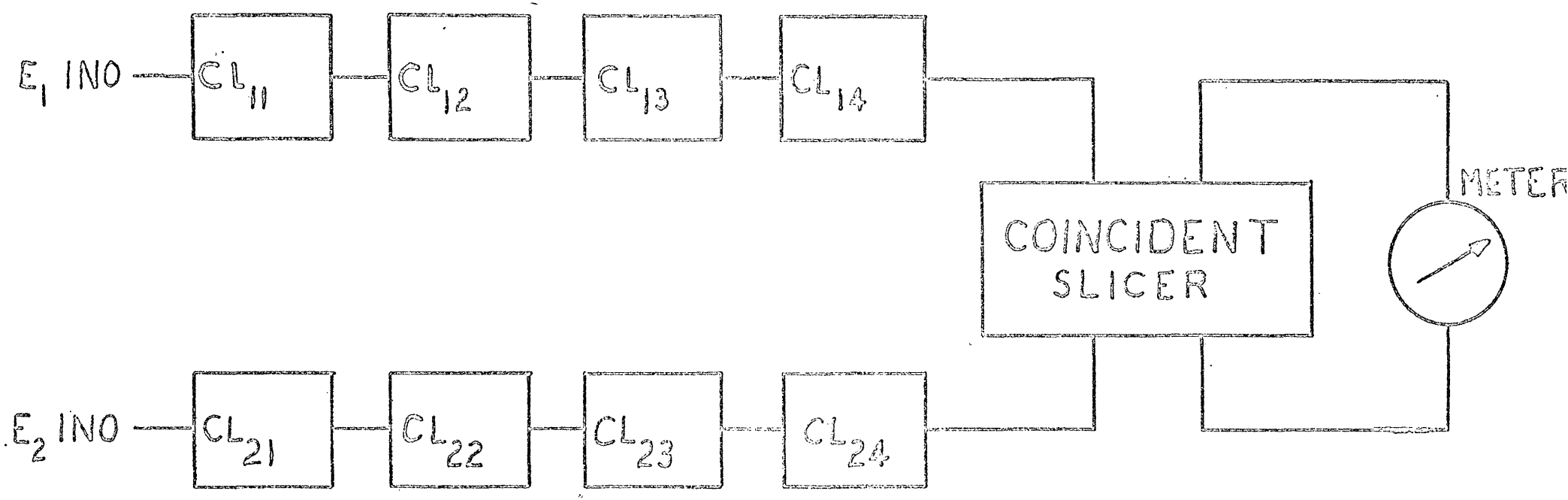
E1 INO
CL11
CL12
CL13
CL14
E2 INO
CL21
CL22
CL23
CL24
COINCIDENT SLICER
METER

FIGURE 15

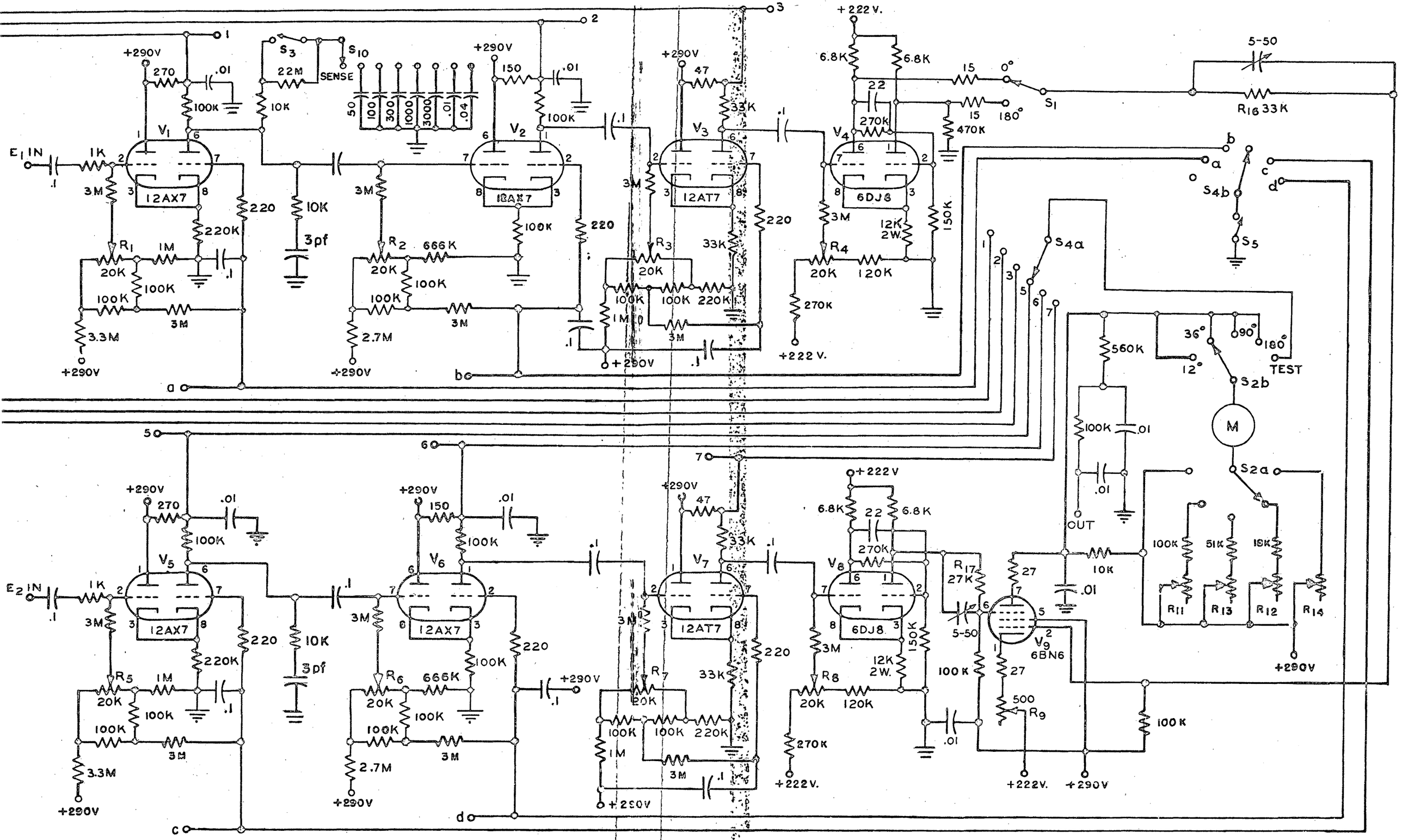

FIG.16 TYPE 405 PHASE METER

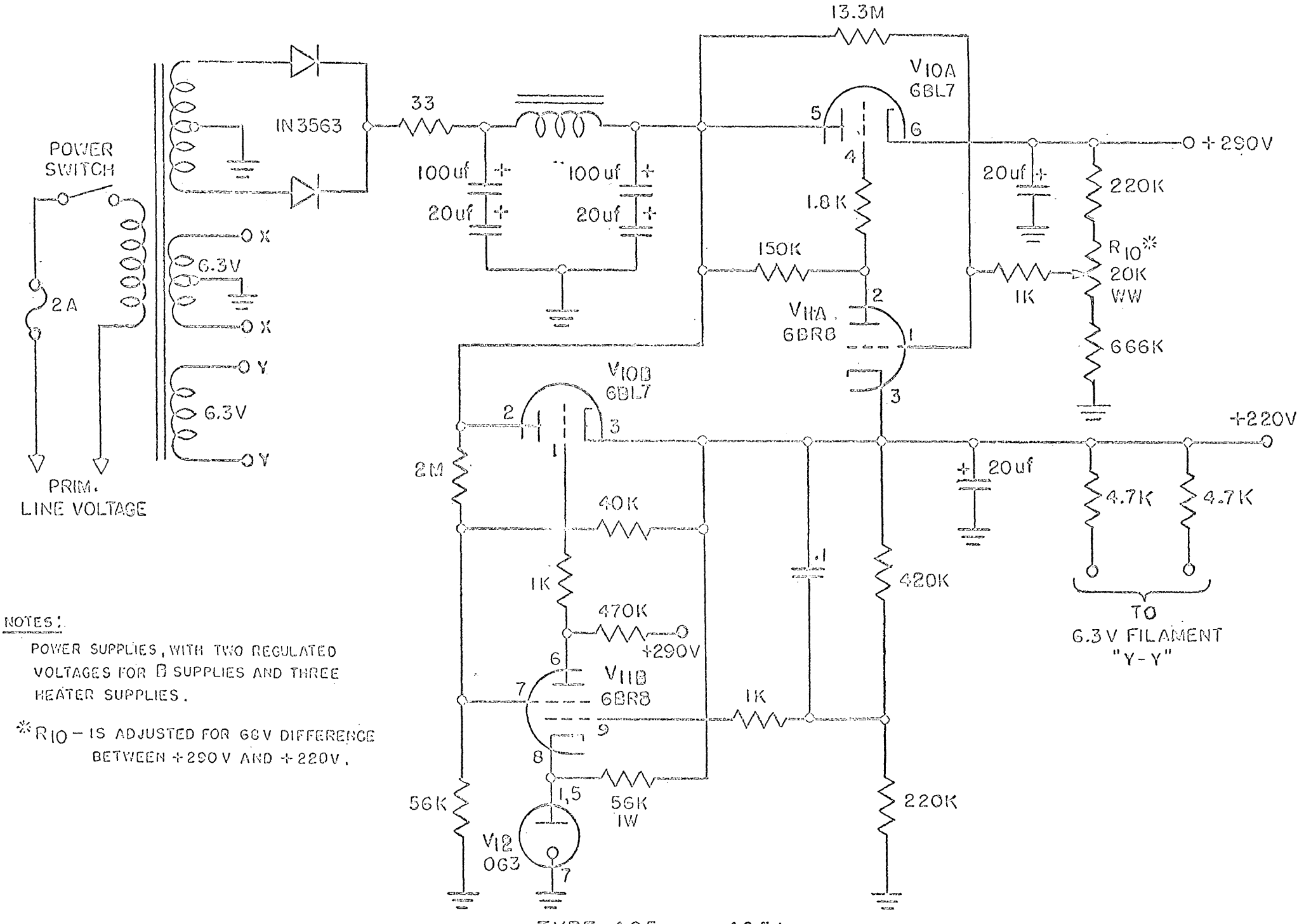

NOTES:

POWER SUPPLIES, WITH TWO REGULATED VOLTAGES FOR B SUPPLIES AND THREE HEATER SUPPLIES.

*R_{10} – IS ADJUSTED FOR 68V DIFFERENCE BETWEEN +290V AND +220V.

TYPE 405 AND 405L
REGULATED POWER SUPPLY
FIG.17.

5.23.63.

studies, the signal from the integrator is fed into the D.C. amplifier and then recorded.

Integrator

The cathode follower and integrator circuit are shown in Figure 18. The cathode follower power supply is shown in Figure 19. This system is used for amplitude scintillation studies and is installed between the detector of the Collins receiver and the recording system. The integrator is used to prevent amplification of frequencies higher than the linear response of the recording system, and the cathode follower presents a constant impedance to the detector of the receiver regardless of recorder time constant. It consists of one-half of a 12AX7, has a gain of one, and a maximum input voltage of about 2.0 volts.[46] In order to preserve the phase and amplitude of the input signal to within five percent, the RC integrator time constant must be less than 1/16 of the minimum period of fluctuation.[47]

Auxiliary Equipment

Since only two 51J-4 Collins Receivers were available, a Hallicrafters SX-62A was to be used for the simultaneous amplitude studies.

A Specific Products Model SR-7R Receiver, built for receiving transmissions from the National Bureau of Standards station WWV, was used to provide time signals. The WWV transmissions are recorded on one channel of the Brush oscillograph simultaneously with the phase and amplitude variations during the satellite transit.

S-66 Satellite

The Polar Ionospheric Beacon Satellite, S-66, is to be placed in orbit for purposes of ionospheric research. The objective set

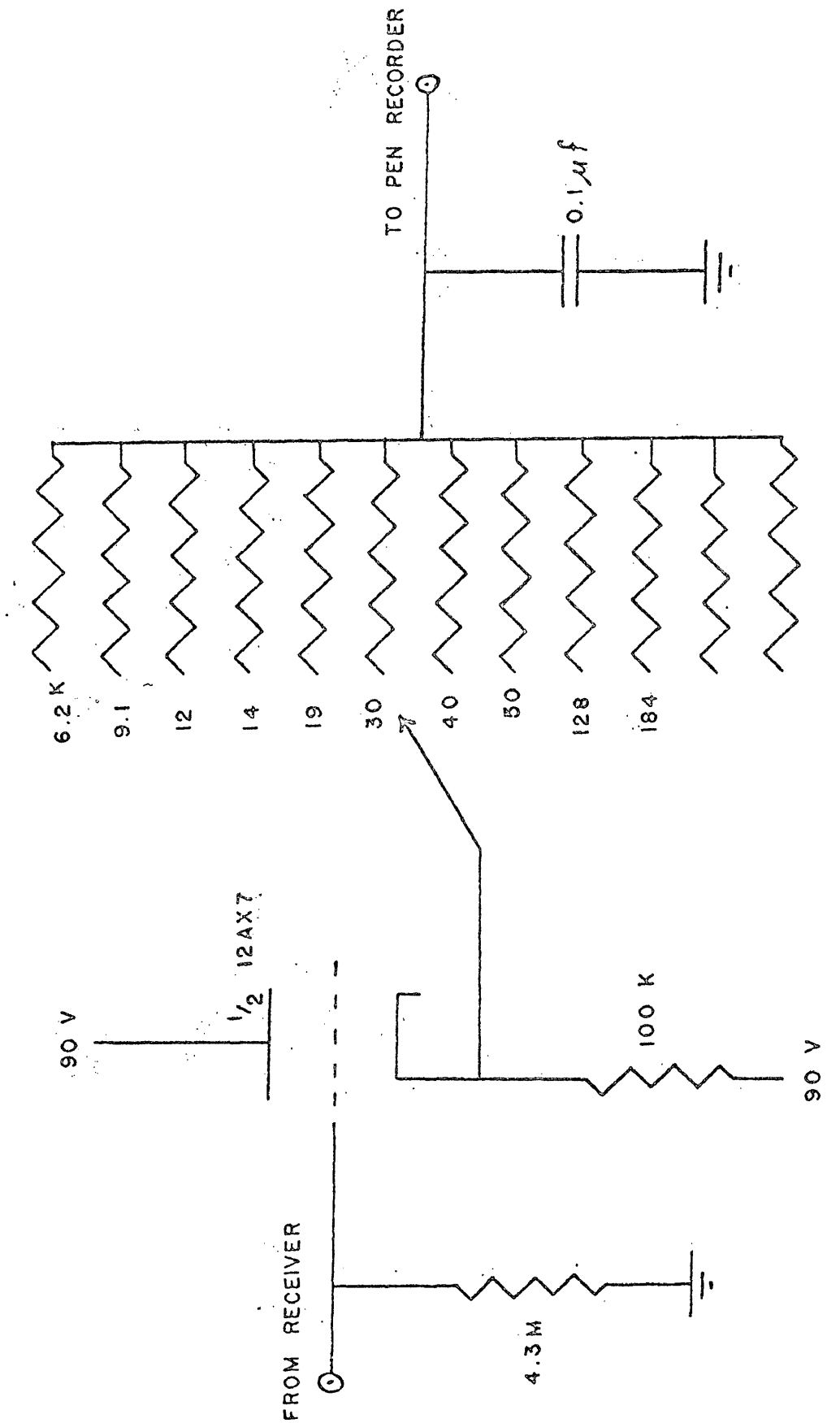

FIGURE 18 CATHODE FOLLOWER AND INTEGRATOR

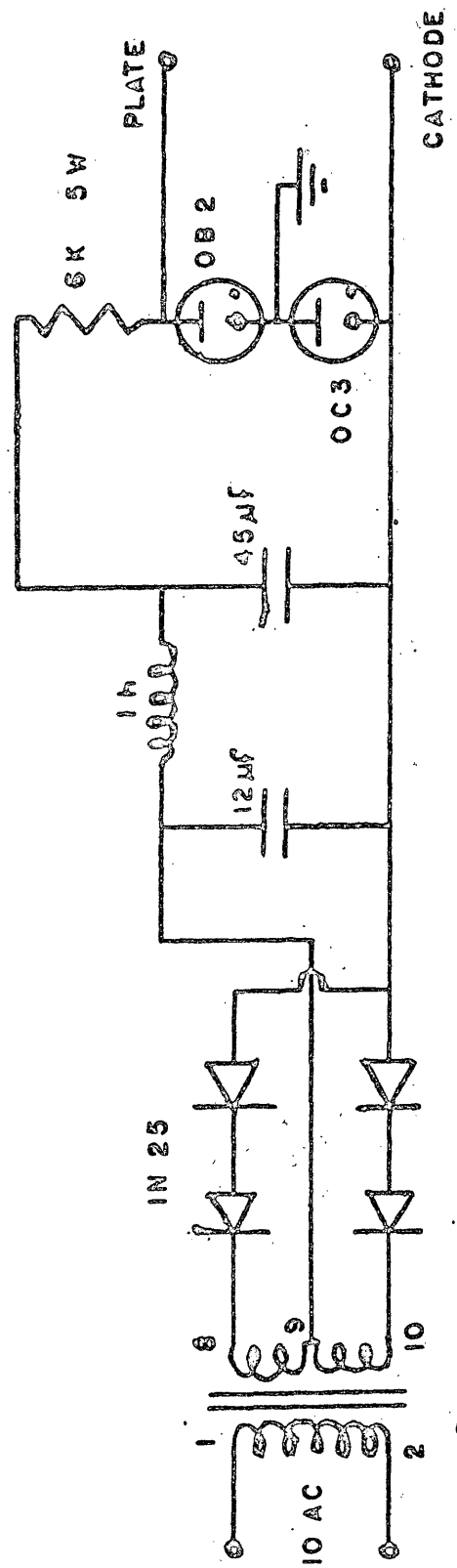

FIGURE 19 POWER SUPPLY

forth for this satellite are:

(1) to determine the total electron content of the ionosphere and to study its diurnal and seasonal variations (to be done under quiet and disturbed conditions),

(2) to provide the means for plotting the total configuration of the ionosphere,

(3) to study the effects of solar flares and the behavior of the ionosphere to solar radiation responsible for producing the ionization,

(4) to determine the geometry and occurrence of irregularities in radio-wave propagation,

(5) to test a newly devised laser tracking system

It was originally to be launched by a Scout launch vehicle which is a four-stage solid-fuel rocket system. It is 72.58 feet long with a body diameter of 3.33 feet and has its propulsion motors arranged in tandem. This system developed extensive trouble, so an attempt was made in March 1964 to use a Delta launch vehicle whose third stage failed to operate properly, making the launch unsuccessful. Thus, at this time, the S-66 has failed to be put into orbit.

The external configuration of the S-66 Satellite is in the shape of a right octagonal prism (see Figure 20) approximately 18 inches across and 12 inches high. It weighs nearly 114 pounds. The power system employs solar cells charging a bank of nickel-cadmium batteries. The solar cells are mounted on four blades which extend outward from the satellite. The power load is 13.24 watts maximum. The ionospheric beacon transmitter system consists of four CW transmitters operating continuously at 20, 40, 41, and 360 MC/S, with the output power of the first three being 250 milliwatts and the 360 MC/S signal being 100

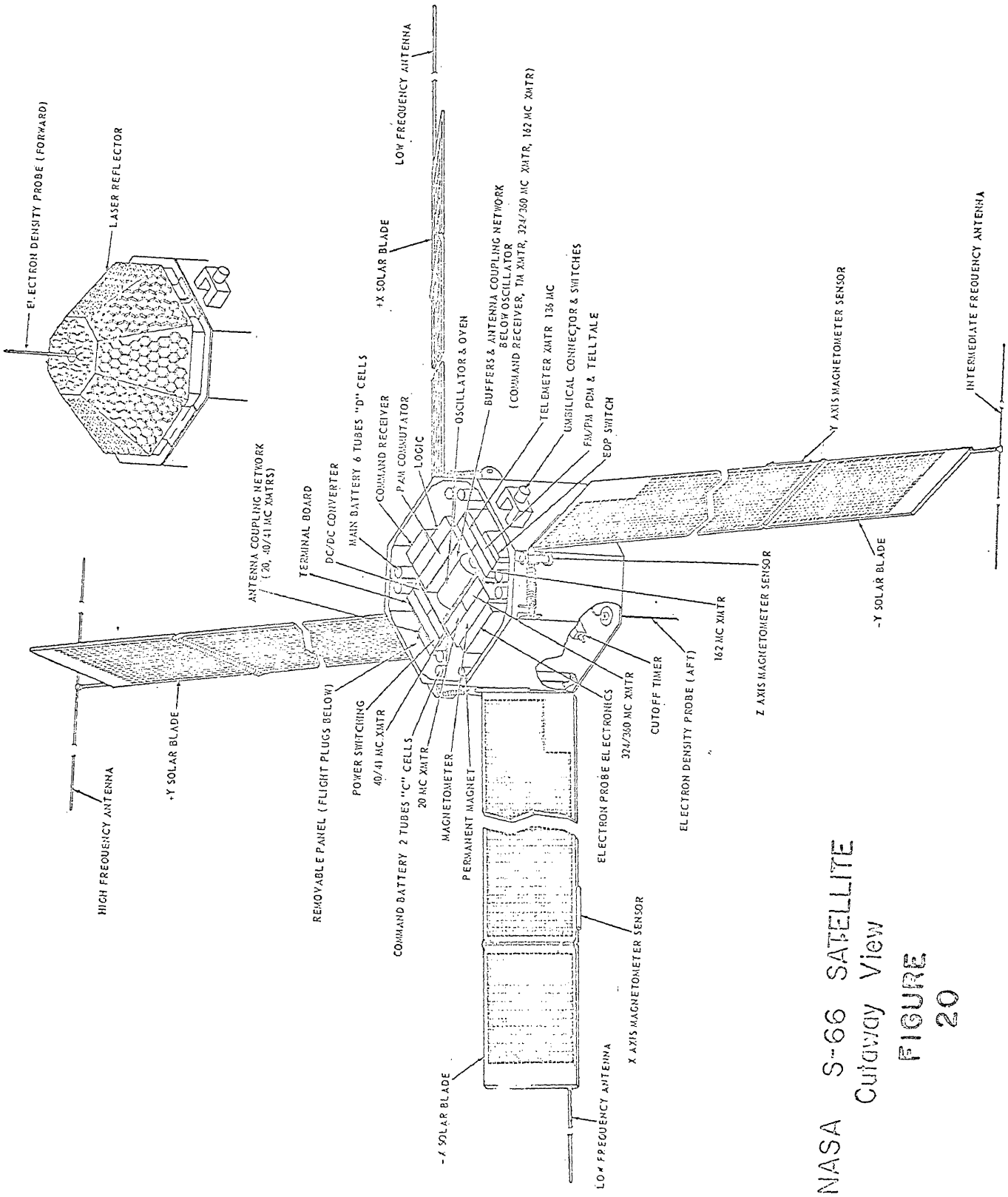

NASA S-66 SATELLITE
Cutaway View
FIGURE
20

milliwatts. The amplitude stability is excellent with a drift less than 2 db per 10 minutes and a frequency accuracy within $\pm$ 0.005%. An A.P.L. Doppler system at 162 and 324 MC/S and a telemetry-transmitter at 136 and 170 MC/S are also contained in the S-66. The antennas for the 20, 40, and 41 MC/S transmissions are 5 feet whip antennas mounted at the end of two oppositely oriented blades.

REFERENCES

1. Jackson, J. E., J. Geophys. Res. 59, 377 (1954)
2. Seddon, J. C., Pickar, A. D., and Jackson, J. E., J. Geophys. Res. 59, 513 (1954)
3. Brest, G. and Tuve, M., Phys. Rev. 28, 554 (1926)
4. Little, C. G., and Lovell, A. C. B., Nature 165, 423 (1950)
5. Aiken, A. C., Ionospheric Research Report No. 133, Penn. State Univ. (1960)
6. Bracewell, R. N., and Bain, W. C., J. Atmos. and Terr. Phys. 2, 216 (1952)
7. Gardner, F. F., and Pawsey, J. L., J. Atmos. and Terr. Phys. 3, 321 (1953)
8. Fejer, J. A., J. Atmos. and Terr. Phys. 7, 322 (1955)
9. Nicolet, M. and Aiken, A. C., J. Geophys. Res. 65, 1469 (1960)
10. Mitra, S. K., The Upper Atmosphere, New York, (1952)
11. Budden, K. G., Radio Waves in the Ionosphere, Cambridge, (1961)
12. Wulf, O. R. and Deming, L. S., Terr. Mag. and Atmos. Elect., 43, 283 (1938)
13. Mitra, S. K., Bhor, J. N., and Ghosh, B. N., Ind. Journ. of Phys. 12, 455 (1938)
14. Nicolet, M., Mem. Inst. Roy. Metenol., Belgium 19, 124 (1945)
15. Bates, D. R. and Hoyle, J. F., Terr. Mag. 54, 51 (1948)
16. Appleton, E. V., and Lyon, A. J., Phys. Soc. (London) 20 (1955)
17. Smith, E. K., Nat'l. Bur. Std. Circular, 582 (1957)
18. Appleton, E. V. and Naismith, R., Proc. Phys. Soc. 52, 402 (1940)

19. Bourdeau, R. E., Space Science Reviews, to be published

20. Martyn, D. F., Proc. Inst. Radio Engrs. 47, 147 (1959)

21. Chapman, S., Proc. Phys. Soc. (London) 43, 26 (1931)

22. Bradbury, N. E., Terr. Mag. and Atmos Elec. 43, 55 (1938)

23. Mohler, F. L. Bur. of Std. Jour. of Res. 25, 507 (1940)

24. Bates, D. R., and Massey, H. S. W., Proc. Roy. Soc. (London) 192, 1 (1947)

25. Martyn, D. F., Proc. Roy Soc. (London) 187, 403 (1946)

26. Massey, H. S. W., Paper presented at Lyons Conference (1947)

27. Briggs, B. H., Jour. of Atmos. and Terr. Phys. 26, 1 (1964)

28. Rangasivamy, S. and Kapasi, K. B., Jour. of Atmos. and Terr. Phys. 25, 721 (1963)

29. Briggs, B. H. and Parkin, I. A., Jour. of Atmos. and Terr. Phys. 25, 339 (1963)

30. Chernov, L.A., Wave Propagation in a Random Medium, McGraw-Hill (1960)

31. Mercier, R. P. Proc. Camb. Phil. Soc. 58, 382 (1962)

32. DeBarber, J. P., Ionospheric Research Report No. 169, Penn. State Univ. (1962)

33. Yeh, K. C., Jour. of Res. of the Nat'l. Bur. of Std. 66D No. 5 (1962)

34. Karavainikov, V. N., Akust. Zh. 3, 175 (1957)

35. Booker, H. G., Proc. of the I.R.E. 46, 298 (1958)

36. Lawrence, J. D., Jr., and Martin, J. D., Jour. of Geophys. Res. 69, 1293 (1964)

37. Bowles, K. L., Cohen, R., Ochs, G. R. and Balsley, B. B., Jour. of Geophys. Res. 65, 1853 (1960)

38. Bowles, K. L. and Van Zandt, T. E., Jour. of Geophys. Res. 65, 2627 (1960)

39. Bowles, K. L., Cohen R. and Calvert, W., Jour. of Geophys. Res. 67 965 (1962)

40. Bowles, K. L., Balsley, B. B. and Cohen, R., Jour. of Geophys. Res. 68, 2485 (1963)

41. Bowles, K. L., and Cohen, R., Jour. of Geophys. Res. 68, 2503 (1963)

42. Deardon, E. W., A.F.C.R.L. - 62 - 350

43. Bowles, K. L., Cospar N62-15191

44. Cahill, L. J., Jr., Jour. of Geophys. Res. 64, 489, 1959

45. Radio Amateurs Handbook, (The American Radio Relay League, 1964), edition 41, 363

46. Lawrence, J. D., Jr., Doctors Dissertation, Univ. of Va. 19

47. Bowhill, S. A., Ionospheric Research Report No. 89, Penn. State Univ. (1956)

APPENDIX I

	Booker	Yeh	Briggs & Parkin
MIDNIGHT MAXIMUM	Midnight max. Electromagnetic damping of turbulence	Midnight max. (No explanation)	Midnight max. (No explanation)
ANISOTROPY OF IRREGULARITIES	No comment	More scintillation when irregularities are longwise along magnetic field lines. (Theoretical)	More scintillation when irregularities are longwise along magnetic field lines. (Theoretical & Experimental)
ZENITH EFFECT	Increase of radio star scintillation with increasing zenith angle. (No explanation)	Increase of satellite zenith angle causes relatively little change in scintillation for temperate latitudes. At low latitudes, it does increase scintillation. (Theoretical, Experimental, & Descriptive)	Increase of radio scintillation with increasing zenith angle with a maximum found at the compliment of the dip angle toward the equation. (Theoretical & Experimental)
SEASONAL VARIATION	Australian workers find a max. at the solstices and a min. at the equinox. Little seasonal variation in northern hemisphere. (No explanation)	Little seasonal variation (No explanation)	No comment
MIDDAY MAXIMUM	Weak midday max. in Australia (No explanation)	No comment	No comment

	Booker	Yeh	Briggs & Parkin
SPREAD-F	Correlation between spread-F and star scintillation. (No explanation)	Correlation between spread-F and satellite scintillation. (No explanation)	Doubt the effectiveness of spread-F on causing scintillation. (Experimental & Descriptive)
HEIGHT VARIATION OF AMPLITUDE SCINTILLATION INDEX	For large irregularities close to the receiver are relatively unimportant for amplitude fluctuations. (Theoretical)	Amplitude scintillation index varies monotonically with height. (Theoretical & Experimental)	A max. is reached when $z_1 = z_2$. (Theoretical)
HEIGHT VARIATION OF PHASE SCINTILLATION INDEX	No comment	Phase scintillation increases to a max. at the top of the slab and then decreases slightly. (Theoretical)	No comment

APPENDIX 2

TABLE

SUMMARY OF EFFECTS OF SOLAR RADIATION ON UPPER ATMOSPHERIC GASES

Spectral region (μ)	Reaction	Height (km)	Remarks
0.300–0.210 (Hartley absorption bands)	$O_3 + h\nu \rightarrow O_2 + O^*$ (excited)	50–60	Strong absorption by ozone. Although the reaction takes place for absorbed radiation with wavelengths $<1.1340\ \mu$, ozone absorbs strongly only from 0.300 to 0.210 μ.
0.1925–0.1760 (Runge Schumann absorption bands)	$O_2 + h\nu \rightarrow O_2^*$ (excited) $\rightarrow 2O$ $O_2^* + O_2 \rightarrow O_3 + O$ $O + O_2 + M \rightarrow O_3 + M$	50–80	Comparatively weak absorption. Sequence of ozone formation.
0.1751–0.1200 (Runge Schumann continuum)	$O_2 + h\nu \rightarrow O + O^*$ (excited)	80–110	Strong absorption. Dissociation of O_2.
0.12157 (Lyman α)	$NO + h\nu \rightarrow NO^+ + e$	60–90	Formation of D region?
0.10247 (Lyman β)	$O_2 + h\nu \rightarrow O_2^+ + e$	90	Contribution to base of E region.
0.1012–0.0910	$O_2 + h\nu \rightarrow O_2^+ + e$	50–80	Weak absorption. Contribution to D region.
0.0910–0.0795	$O + h\nu \rightarrow O^+ + e$	>200	Very strong absorption. Ionization of O contributes to F_1 and F_2 regions?
0.0795–0.0755	$N_2 + h\nu \rightarrow N_2^+ + e$	140–160	Comparatively weak absorption. Contribution to E_2 region?
0.0744–0.0661	$O_2 + h\nu \rightarrow O_2^+$ (excited) $+ e$	90–120	Strong absorption. Contribution to E_1 region?
0.0661–0.0585	$N_2 + h\nu \rightarrow N_2^+$ (excited) $+ e$	200	Very strong absorption. Contribution to F_1 region.
2×10^{-2}–1.5×10^{-3} (X-rays)	General ionization	90–150	Contribution to E and F regions.
$\sim 2.5 \times 10^{-4}$	General ionization	60–90	Contribution to D region?

[a] Based on S. K. Mitra, *Compendium Meteorol.*, p. 245 (1951), and H. Friedman, in *Physics of the Upper Atmosphere* (J. A. Ratcliffe, ed.), p. 133. Academic Press, New York, 1960.

VITA

Michael Patrick McCormick

Born in Canonsburg, Pennsylvania, November 23, 1940. Graduated from Canonsburg High School, June 1958; B. A. in physics, Washington and Jefferson College, 1962. Served with the United States Bureau of Mines, Health and Safety Activity, Pittsburgh, Pennsylvania, summer of 1962. Entered the College of William and Mary as a Ph.D. candidate in physics, September 1962.